PHILOSOPHICAL TRANSACTIONS OF THE ROYAL SOCIETY B BIOLOGICAL SCIENCES

Probabilistic Secretion of Quanta at Somatic Motor-Nerve Terminals: The Fusion-Pore Model, Quantal Detection and Autoinhibition

P. C. Thomson, N. A. Lavidis, J. Robinson and M. R. Bennett

Phil. Trans. R. Soc. Lond. B 1995 **349**, 197-214
doi: 10.1098/rstb.1995.0103

Probabilistic secretion of quanta at somatic motor-nerve terminals: the fusion-pore model, quantal detection and autoinhibition

P. C. THOMSON[1]*, N. A. LAVIDIS[2], J. ROBINSON[1] AND M. R. BENNETT[2]‡

The School of Mathematics and Statistics[1] and The Neurobiology Laboratory[2], Department of Physiology, University of Sydney, N.S.W. 2006, Australia

CONTENTS

SUMMARY

The probability of detecting first, second, and later quanta secreted at release sites of a motor-nerve terminal during the early release period following a nerve impulse has been addressed. The possibility that early quantal release autoinhibits later quantal release during this period has also been ascertained. In this investigation, a model for the secretion of a quantum at a release site is developed in which, following the influx and diffusion of calcium ions to a release site protein associated with synaptic vesicles, k steps of association of the ions with the protein then occur at rate α. The release site protein then undergoes a conformational change which may not go on to completion if calcium ions dissociate from the protein at rate γ. If this process does reach completion then a fusion-pore between the vesicle and the presynaptic membrane is created; this happens at rate δ. Key assumptions of this fusion-pore model are that the

* Present address: Biometry Unit, Department of Crop Sciences, University of Sydney.
‡ To whom correspondence should be sent.

quantal secretions from each site are independent of each other, and that there is a large number of vesicles, each with a small probability of secretion, so that the number of secretions is Poisson in nature. These assumptions allow analytical expressions to be obtained for predicting the times at which first, second and later quanta are secreted during the early release period following an impulse.

To test the model, experiments were performed in which the times of first, second and later quantal releases were determined at discrete regions along the length of visualized motor-terminal branches in toad (*Bufo marinus*) muscles. Estimates of model rate constants and of k from the times for first quantal secretions failed to give satisfactory predictions of the observed times of later secretions. Therefore, either the model fails, or the procedure used for detecting later quantal events as a consequence of their being masked by earlier quantal events is inadequate.

To solve this detection problem, a two-dimensional analysis of the spread of charge following the secretion of a quantum at a random site on the motor-terminal branch has been done. This allows determination of the probability that later quanta will be detected following secretion of earlier quanta. The detection model was then incorporated into the fusion-pore model to predict the times at which second and later quanta occur during the early release period, based on the estimates of the model parameters derived from the analysis of first quantal releases. Good estimates were now obtained for the observed times of second and later quantal releases, indicating that appropriate procedures must be adopted for adequate detection of quantal secretions. Furthermore, the experiments provide support for the fusion-pore model.

It has been suggested that the binomial nature of quantal release from the entire motor-nerve terminal may be explained if early quantal release inhibits later quantal release during the early quantal release phase (M. R. Bennett & J. Robinson 1990, *Proc. R. Soc. Lond.* B **239**, 329–358). Although the fusion-pore detection error model gave good predictions of the observed times of first, second and later quantal releases, these may be improved if a model for autoinhibition is included. In this model the first quantum was taken as giving rise to an inhibition of secretion that propagates to surrounding release sites with a constant velocity, v. A combined model incorporating the fusion-pore detection error model and that for autoinhibition was then used to predict second and later quantal latencies, by using the first quantal latencies to determine the estimates for the parameters in the combined model. When this analysis was done on the times for quantal secretion at sites on thirteen different motor-nerve terminals, the value of v was estimated as zero in each case, so that no autoinhibitory effect was observed.

1. INTRODUCTION

Katz & Miledi (1965*a*) obtained the first histogram of the latency of quantal secretion following a nerve impulse at a restricted number of release sites of somatic motor-nerve terminals. At room temperature the earliest quantal secretion did not occur until a time (τ), about 0.5 ms after the impulse, with the rate of secretion reaching a maximum within a millisecond and then declining approximately exponentially within about 3.0 ms. Stevens (1968) explicitly identified that there was an underlying stochastic process governing this time course, in which the nerve impulse initiated a quantal release process (with a rate $\alpha(t)$) at each of the n release sites. The probability of quantal secretion in the interval $(t, t+\mathrm{d}t)$ is then $\alpha(t)\,\mathrm{d}t$ approximately (for small $\mathrm{d}t$), and the total release rate is $\lambda(t) = n\alpha(t)$. Using this formulation Barrett & Stevens (1972*a*, *b*) showed that $\alpha(t)$, determined from the latencies of first quantal secretions following an impulse, declined exponentially over a wide range of temperatures. Bennett *et al.* (1977) showed that the observed distribution of quantal latencies from release sites (T) could be reasonably well described by a gamma random variable with parameters (α, k) for time to release, coupled with an exponential random variable (with parameter γ) for the site becoming unavailable for release. Under this model, the probability of secretion of a quantum at one of the n release sites is $[\alpha/(\alpha+\gamma)]^k$.

There are three main events involved in the process of quantal secretion. Firstly, calcium ions must enter through voltage-dependent calcium channels and diffuse to the sites of vesicle exocytosis (Yamada & Zucker 1992; Parnas *et al.* 1989). Secondly, calcium ions bind to a release site protein which may be responsible when activated for generating a tension that brings the vesicle and presynaptic membrane together so that an early lipid fusion-pore forms between the two membranes (Monck & Fernández 1992; Nanavati *et al.* 1992). Alternatively, the calcium ions may bind to a fusion-pore protein that already joins the vesicle to the release site, with subsequent opening of the protein channel (Almers 1990). Finally the lipid fusion-pore can expand irreversibly (Oberhauser *et al.* 1992), or lipids can invade the subunits of the open channel leading to irreversible expansion of the channel (Almers 1990); in either case exocytosis occurs. It is natural to ascribe the different components of the stochastic process to dfferent elements of the secretion process. In this case, the influx of calcium and its diffusion to the release site protein is associated with the minimum latency (τ) as originally suggested by Katz & Miledi (1965*b*); at a temperature of 3 °C this is about 5 ms. The binding of calcium ions at rate α to k different sites on the release protein, with the probability of a bound calcium ion becoming dissociated at rate γ, may then be described by the gamma variate T with parameters $(\alpha+\gamma, k)$, responsible for the overall shape of the quantal secretion

PHILOSOPHICAL TRANSACTIONS OF THE ROYAL SOCIETY B BIOLOGICAL SCIENCES

histogram. Although estimates for the rate constants α and γ are not yet available for the release protein, rate constants for the process that stops the release (γ) are probably about 1 ms^{-1} at less than 10 °C (Yamada & Zucker 1992). Finally, the irreversible opening of the fusion-pore may be associated with the exponential variate U with parameter δ. This might be large, as at room temperature the rate is likely to be of the order of 10 ms^{-1} (Almers *et al.* 1989). Conditional on their being no dissociation, the expected value for the time to secretion (W) is

$$E(W) = k/(\alpha+\gamma)+1/\delta.$$

If δ is large then the calcium reaction with the release site protein is rate limiting, and this step may be ignored in analyses; if δ is small, then the rate of exocytosis becomes limiting (Bennett & Robinson 1990). The Q_{10} of the minimum delay is high (about three; Katz & Miledi 1965*b*), as are the subsequent delays that make up the histogram of the latencies of quantal secretions (Katz & Miledi 1965*b*; Barrett & Stevens 1972*b*; Bennett *et al.* 1977; but see Van der Kloot 1988*b*). This is to be expected if τ is governed by the kinetics of opening and closing of voltage-dependent calcium channels, with T dependent on the rates of reaction with the release site protein ($\alpha+\gamma$), and U on the rate of irreversible opening of the fusion-pore (δ). To obtain estimates for these parameters from both first and second quantal latencies, as well as from the interval between them, analytical expressions have been obtained for these probability distributions in the first part of the present work, and maximum likelihood techniques used to derive these estimates.

Although Barrett & Stevens (1972*a*) found in most cases no significant effect of first quantal secretion on the probability of a second quantal secretion to the same stimulus, they did obtain evidence for initial depressive interactions on some occurrences, especially at sites that had been previously active. Depressive interactions were studied in detail by Baldo *et al.* (1986). They found significant differences in the value of α determined from second quantal latencies ($\alpha_2(t)$) compared with that from the first quantal latencies ($\alpha_1(t)$), indicating that the probability of secretion for the second quanta was different from that of the first quanta; the estimate of $\alpha_2(t)$ was lower during the first few milliseconds of the evoked secretion period relative to $\alpha_1(t)$. The problem of detecting second or later quantal secretions, as a consequence of their being obscured by the first quantal secretion, has been pointed out by these authors but no analytical technique has yet been proposed to cope with this difficulty. As a consequence it is unclear whether depressive initial effects do occur between quantal secretions. In the second part of this work, an analytical procedure is developed that allows for this detection error in the counting of second quantal secretions.

The somatic motor-nerve terminals possess hundreds of release sites from which quanta can be secreted on arrival of the nerve impulse (Katz 1969). If the quantal content of the endplate potential is used as a measure of secretion from all these sites, then this does not fluctuate much at secretion rates just subthreshold for the initiation of the muscle action potential. The quantal secretion has a variance smaller than its mean, contrary to what is expected for a Poisson random variable (Bennett & Florin 1974; Wernig 1975; Bennett & Fisher 1977). The discovery that different release sites have markedly different probabilities for the secretion of a quantum (Bennett & Lavidis 1979; D'Alonzo & Grinnell 1985) would provide an explanation for the small variance in quantal secretion if a few of these sites had high probabilities and the rest had very low probabilities (Bennett & Fisher 1977), but this is not the case; although very low probability sites do exist among high probability sites (Bennett & Lavidis 1989), there are relatively large numbers of high probability sites along the length of the terminal branches (Bennett *et al.* 1986). An alternative explanation for the small variance in quantal secretion depends on the existence of inhibitory influences that propagate from a release site on secretion of a quantum. For example, substances are secreted with the transmitter that may mediate interaction between adjacent release sites following the secretion of a quantum (Jones 1987), although the rate and range of diffusion of such substances is likely to limit their effects during the secretion period to very few sites. Nevertheless, activation of autoreceptors by these substances may lead to a decline in the probability of secretion from adjacent sites following quantal secretion from a particular site. If this does occur within the early secretion period following a nerve impulse it would lead to an initial depression of quantal secretion as well as a decrease in the variance of quantal secretion (Bennett & Robinson 1990). This is investigated in the present work by using the detection theory to determine if the probabilistic secretion of second quanta ($\alpha_2(t)$) is in any way depressed by the prior secretion of the first quanta ($\alpha_1(t)$).

2. METHODS

(*a*) *Housing of animals*

Toads (*Bufo marinus*) ranging in length from 55 to 70 mm from tail to nose were maintained in a room that was fitted with 15% ultraviolet lights. Lights were turned on for 16 h per day. The temperature of the room was maintained between 25 and 30 °C and the animals were fed two times per week with a mixture of minced meat and fish brittle.

(*b*) *Tissue preparation*

Animals were anaesthetized with tricaine methanesulphonate (MS222, Rural Chemical Industries Australia) and then killed by a cervical fracture. The right iliofibularis muscle with its nerve supply was dissected from its surrounding connective tissue and cut at its tendinous insertions. The muscle was then pinned to Sylgard on the bottom of a 3 ml organ bath with the surface where the nerve enters the muscle facing up. The muscle was stretched to approximately 110% of its resting length in the limb to form a flat parallelogram. The preparation was continuously perfused at the rate of 5 ml min^{-1} with a modified

Ringer solution containing (mM): Na^+, 117.0; K^+, 3.0; Mg^{2+}, 10.0; Cl^-, 122.7; $H_2PO_4^-$, 1.3; HCO_3^-, 16.3; Ca^{2+}, 0; glucose, 7.8. The temperature of the bath was maintained between 1 and 4 °C. The reservoir supplying the bath was continuously gassed with 95% O_2 and 5% CO_2, and the pH was maintained between 7.2 and 7.5.

(*c*) *Visualization of the nerve terminal*

The preparation was left bathing in zero extracellular calcium ion concentration for about 40 min while contractions due to nerve stimulation diminished. The muscle was then bathed for 30 s in 3,3-diethyloxardicarbocyanine iodide ($DiOC_2(5)$, 0.1 mM; Yoshikami & Okun 1984) and then washed with Ringer for 10 min to fluorescently label accumulations of mitochondria corresponding to the nerve terminal branches. Excitation at 560 nm of the $DiOC_2(5)$ resulted in a fluorescence that was visible with use of a Rhodamine filter set (Olympus BH2 microscope). Terminals were chosen by viewing the fluorescent image via an image intensifier camera (National) on a video monitor (National). To avoid long periods of fluorescing the preparation and the need for repeated applications of $DiOC_2(5)$, the image of the fluorescing terminals was traced onto the video monitor screen (see Bennett *et al.* 1986).

(*d*) *Stimulation*

The iliofibularis nerve was gently sucked into a pipette filled with the Ringer solution. It was then stimulated by using square wave current pulses of 0.08 ms duration and 8 V amplitude. At least 200 samples of evoked release were recorded at 0.5 Hz for each electrode placement.

(*e*) *Recording*

Extracellular recordings of the endplate current were obtained by using microelectrodes filled with Ringer solution containing zero magnesium ions and 10.0 mM calcium ions. The tip diameter of the recording electrodes was about 2 μm. Focal extracellular recordings were obtained by placing the electrode about 2 to 3 μm to one side of the terminal branch. The intra-electrode solution was allowed to diffuse freely out of the electrode forming a stream that flowed over the terminal branch in the direction of flow of the bathing solution. The extent of spread of the intra-electrode solution over the terminal branch was determined by the direction and flow rate of bathing solution. The external signs of the endplate current could then be observed on the oscilloscope screen while the nerve was stimulated. In most cases small endplate potentials could be seen within 20 impulses. The electrode was then lifted off the muscle fibre and moved in either direction along the same axis as the terminal branch until the source of these small endplate currents was located (this procedure involved searching for the most active release site). The external electrode was then lifted again off the muscle fibre and moved transversely to improve the recording of the nerve impulse. Two hundred samples of the evoked release over 7 min were recorded.

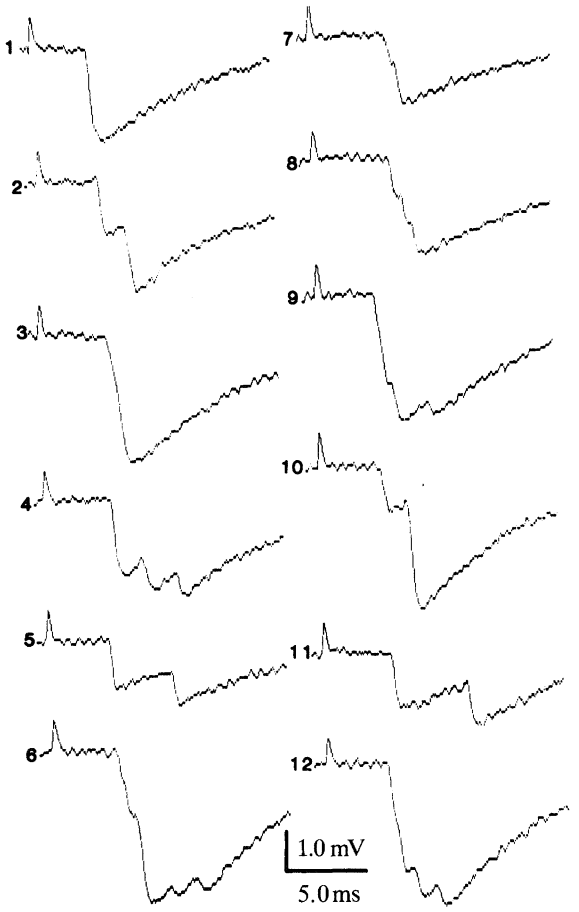

Figure 1. Focal extracellular recordings of endplate potentials taken from a proximal site on a $DiOC_2(5)$ visualized motor-nerve terminal. The temperature was 7.0 °C. The numbers refer to the particular trial during stimulation of over 200 trials.

Endplate currents were recorded by using focally placed electrodes and collected on an IBM-AT microcomputer with use of p-clamp software (Axon Instruments). Examples of recorded extracellular potentials are shown in figure 1. To be able to measure potentials from individual quanta, the preparation was kept between 1 and 4 °C. Since the background rate of spontaneous potentials was very low, it would not adversely affect results by assuming all the quantal secretions were from evoked potentials.

3. THE FUSION-PORE MODEL OF QUANTAL SECRETION

In this section, the probability distributions for time till first and second quantal secretions, together with the interval between them, will be derived by using the fusion-pore model.

Consider a branch of a neuron terminal with a finite number of release sites, n, at locations $x_1, x_2, \ldots, x_n$, assumed to lie in the interval $[0, 1]$. As indicated in

PHILOSOPHICAL TRANSACTIONS OF THE ROYAL SOCIETY B BIOLOGICAL SCIENCES

Bennett & Robinson (1990) (their equation (1)), the cumulative probability of the time to release for the site at x_i is given by the gamma form,

$$p(x_i, t) = \left(\frac{\alpha(x_i)}{\alpha(x_i)+\gamma}\right)^k G(t; \alpha(x_i)+\gamma, k),$$

where $\alpha(x_i)$ is the rate of calcium ion binding in the release site located at x_i, k is the number of binding steps and γ is the dissociation or failure rate of the process. $G(t; \alpha(x_i)+\gamma, k)$ is the cumulative distribution function of a gamma random variable with parameters $(\alpha(x_i)+\gamma, k)$. If the time for opening of the fusion-pore is also included (an exponential variate with rate δ), this rate should be modified to

$$p(x_i, t) = \left(\frac{\alpha(x_i)}{\alpha(x_i)+\gamma}\right)^k \delta \int_0^t G(t-u; \alpha(x_i)+\gamma, k)\, e^{-\delta u}\, du.$$

If the fusion pore opening time is fast (large δ), then this expression for $p(x_i, t)$ approaches the previous expression. It has been assumed for the model fitting process that the fusion-pore opening is fast. By letting the number of release sites increase to infinity and the release probability $p(x_i, t)$ approach zero, the expected number of all quantal secretions up to time t is

$$\Lambda(t) = (\lambda/\gamma)^k G(t; \gamma, k),$$

or

$$\Lambda(t) = \left(\frac{\lambda}{\gamma}\right)^k \delta \int_0^t G(t-u; \gamma, k)\, e^{-\delta u}\, du,$$

fusion-pore opening time being taken into account, where λ^k is defined as the constant, $\lim_{n\to\infty} \Sigma_{i=1}^n \alpha^k(x_i)$, and

$$G(t; \gamma, k) = \int_0^t g(u; \gamma, k)\, du, \quad t > 0,$$

where

$$g(t; \gamma, k) = \frac{\gamma^k}{\Gamma(t)} t^{k-1} e^{-\gamma t}, \quad t > 0.$$

Note that λ is consequently a measure of the calcium binding rate across the entire neuron terminal branch. The expected total number of quantal releases is given by

$$\Lambda(\infty) = (\lambda/\gamma)^k.$$

This expression for $\Lambda(\infty)$ is the same whether or not time for fusion is taken into account. In fact, provided that δ is greater than λ and γ, there is very little difference in the form of the rate functions, $\Lambda(t)$, for all elapsed times, t.

The instantaneous rate is

$$\lambda(t) = (\lambda/\gamma)^k g(t; \gamma, k),$$

or

$$\lambda(t) = \left(\frac{\lambda}{\gamma}\right)^k \delta \int_0^t g(t-u; \gamma, k)\, e^{-\delta u}\, du$$

including the time for fusion, where $\lambda(t)\, dt$ is (approximately) the expected number of secretions in the interval $(t, t+dt)$. The quantal secretion rate is not necessarily constant along the length of the neuron terminal; so the rate may be expressed with a spatial component, $\Lambda(x, t)$, where $\Lambda(x, t)\, dx$ is (approximately) the expected number of quantal secretions up to time t in the element of terminal $[x, x+dx]$. It will be assumed that the time and location of secretion are independent, and so may be expressed as $\Lambda(x, t) = \theta(x)\, \Lambda(t)$, where $\theta(x)$ is the probability density function for the location of the quantal secretion $(0 \leqslant x \leqslant 1)$. A beta form may be used, $\theta(x) = [B(a, b)]^{-1} x^{a-1}(1-x)^{b-1}, 0 \leqslant x \leqslant 1$ (see Bennett & Lavidis 1979). However, when a relatively small length of neuron terminal is investigated, a uniform form $(a = b = 1)$ may be a reasonable approximation, and this will be assumed in the sequel.

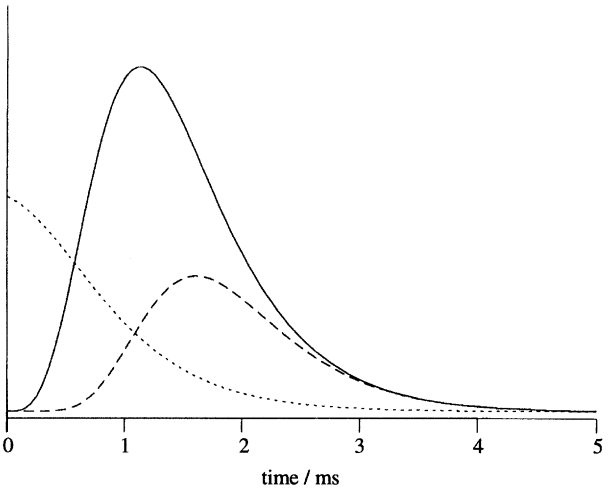

Figure 2. Examples of distributions of T_1 (solid line), T_2 (broken line) and S_1 (dotted line) based on the fusion-pore model. The parameters set for this model were $\lambda = 3$ ms^{-1}, $\gamma = 3$ ms^{-1} and $k = 5$. Note that the area under each curve corresponds to the probability of observing a t_1, t_2 or s_1 in finite time.

The following section outlines the probability density functions and other probability terms for times of quantal secretions. They are shown with the general expressions for $\lambda(t)$ and $\Lambda(t)$. The probability density function for the time until the first release (T_1) is

$$f_{T_1}(t_1) = \lambda(t_1) \exp[-\Lambda(t_1)], \quad t_1 > 0, \tag{1}$$

and an illustration of this distribution is shown in figure 2, along with the other time course distributions. The distribution of T_1 is improper; that is, it does not integrate to one. The probability of no secretions in finite time ($T_1 = \infty$, no first secretion) is

$$P(T_1 = \infty) = \exp[-\Lambda(\infty)]. \tag{2}$$

The conditional probability density function of the second secretion, T_2, given $T_1 = t_1$ is

$$f_{T_2}(t_2 \mid t_1) = \lambda(t_2) \exp\{-[\Lambda(t_2) - \Lambda(t_1)]\}, \quad t_2 > t_1, \tag{3}$$

and the conditional probability of no finite T_2 is

$$P(T_2 = \infty \mid T_1 = t_1) \exp\{-[\Lambda(\infty) - \Lambda(t_1)]\}. \tag{4}$$

The joint probability density function for the distribution of the first two secretions (T_1, T_2) is

$$f_T(t_1, t_2) = \lambda(t_1)\, \lambda(t_2) \exp[-\Lambda(t_2)], \quad t_2 > t_1, t_1 > 0,$$

PHILOSOPHICAL TRANSACTIONS OF THE ROYAL SOCIETY B BIOLOGICAL SCIENCES

Table 1. *Descriptive statistics for the first four releases* (t_i, $i = 1, \ldots, 4$) *and intervals between releases* ($s_i = t_{i+1} - t_i$, $i = 1, \ldots, 3$)

(Units of time are milliseconds.)

	size	mean	s.d.	min.	max.
t_1	696	6.626	0.575	5.46	10.08
t_2	304	7.354	0.683	6.09	10.01
t_3	66	7.868	0.573	6.79	9.66
t_4	6	8.690	0.863	7.34	9.80
s_1	304	0.932	0.530	0.28	3.15
s_2	66	0.960	0.437	0.39	2.38
s_3	6	1.008	0.647	0.41	2.24

and from this the marginal probability density function of T_2 is obtained as

$$f_{T_2}(t_2) = \lambda(t_2)\, \Lambda(t_2) \exp[-\Lambda(t_2)], \quad t_2 > 0.$$

The probability density function of the interval between the first two secretions, $S_1 = T_2 - T_1$, is

$$f_{S_1}(s_1) = \int_0^\infty f_T(t_1, s_1 + t_1)\, \mathrm{d}t_1$$

$$= \int_0^\infty \lambda(t_1)\, \lambda(s_1 + t_1) \exp[-\Lambda(s_1 + t_1)]\, \mathrm{d}t_1, \quad s_1 > 0.$$

For the experimental data analysed, an additional parameter was required, a time lag, τ, to account for the minimum synaptic delay following stimulation. The effect of this is to move the time origin to the right, and so time may be written as $t' = t - \tau$ to reset the time origin at zero (for example, $\lambda(t') = \lambda(t - \tau)$ for $t > \tau$).

(*a*) *Failure of the fusion-pore model to predict second quantal latencies*

Thirteen experimental data sets have been analysed, but detailed results will only be given for the first of these sets, in this model and subsequent ones. A summary of the results of all the data sets will be included later (§6). For the first data set, times of secretion for first, second, third and fourth quanta from the release sites are shown in table 1. These sites had a frequency distribution of the total number of quantal secretions ($f_i; i = 0, \ldots, 4$) $f_0 = 104, f_1 = 392, f_2 = 238$, $f_3 = 60$ and $f_4 = 6$, giving a mean of 1.340 quanta and a variance of 0.680. By using the maximum likelihood procedure (see appendix B), the parameter estimates from the data based on 696 finite t_1 and 104 infinite t_1 were $\hat{\lambda} = 4.96\ \mathrm{ms}^{-1}$, $\hat{\gamma} = 4.60\ \mathrm{ms}^{-1}$, $\hat{k} = 9.44$ and $\hat{\tau} = 4.92$ ms. However, Monte Carlo simulation studies have demonstrated a high degree of linear correlation between these parameter estimates, leading to their unstable estimation. Given that the mean value of $\hat{k}$ for all 13 sets of experimental data was 5.40 (with a standard deviation of 2.88), which was close to the hypothesized number of calcium ion binding steps (five, see §7), k was forced to be equal to five in this and the other twelve analyses of experimental data. When this was done, the parameter estimates changed to $\hat{\lambda} = 3.39\ \mathrm{ms}^{-1}$, $\hat{\gamma} = 2.94\ \mathrm{ms}^{-1}$ and $\hat{\tau} = 5.33$ ms. Inclusion of second release times changed these estimates slightly ($\hat{\lambda} = 3.23\ \mathrm{ms}^{-1}$, $\hat{\gamma} = 3.01\ \mathrm{ms}^{-1}$ and $\hat{\tau} = 5.28$ ms). Based on these estimates, the theoretical distributions of t_1, t_2 and $s_1 = t_2 - t_1$ have been calculated and these along with the histograms of the data are shown in figure 3. The fit of the time till the first quantal secretion is very good, whereas the fit to the second secretion is poor, as is that to s_1. In particular the histogram for s_1 shows that there are no quantal secretions that occur shortly after the first. The good predictions for t_1 but not for t_2 or s_1 were the same for all thirteen experiments. This may be due to the difficulty of detecting two or more quantal secretions that occur in quick succession following a nerve impulse, as previously noted by Barrett & Stevens (1972*a*) as well as Baldo *et al.* (1986). A theory to

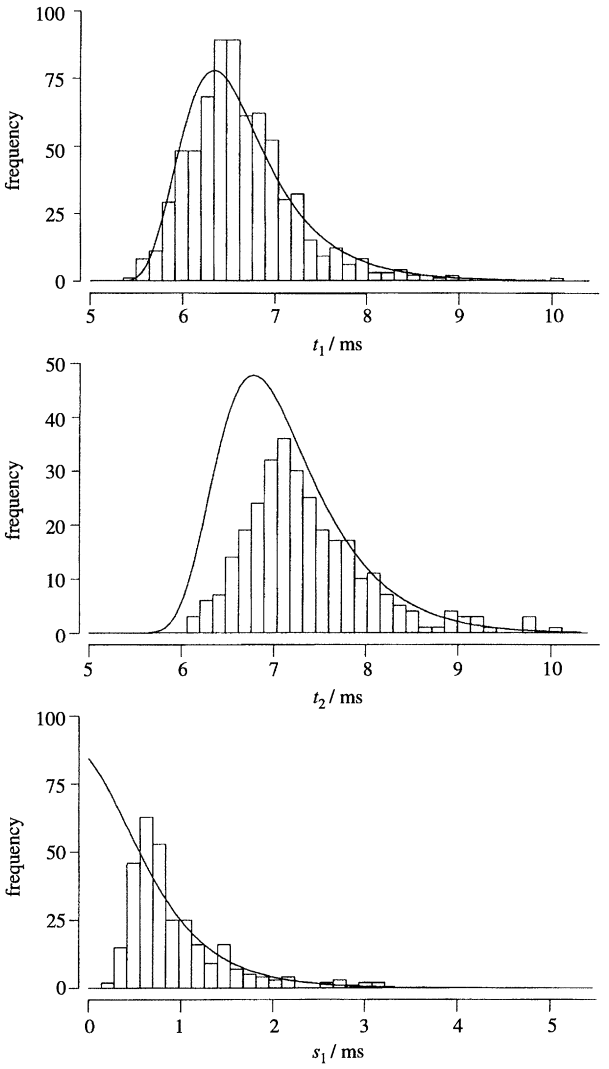

Figure 3. Comparison of the observed times of quantal secretions (histogram) with that of the predicted distributions (solid line) according to the fusion-pore model. Times are for the first quantal secretion (t_1), second quantal secretion (t_2) and the interval between first and second quantal secretions ($s_1 = t_2 - t_1$). Estimates of the parameters in the model were obtained from the first quantal secretion times in experiment 1 ($\hat{\lambda} = 3.39\ \mathrm{ms}^{-1}$, $\hat{\gamma} = 2.94\ \mathrm{ms}^{-1}$ and $\hat{\tau} = 5.33$ ms). The data are also from experiment 1.

account for detection of quanta following the first was therefore developed.

4. THE FUSION-PORE MODEL WITH ALLOWANCE FOR DETECTION OF MULTIPLE QUANTAL SECRETIONS

Experimental evidence indicated that there is a minimum synaptic delay during which no detection is possible and after this, a period in which the signs of quantal secretion may be masked by prior secretions (Katz & Miledi 1965*a*, *b*). The experimental procedure used for detecting a quantal secretion is to determine the time at which the endplate potential *starts* to increase towards a maximum; however if the start of increase of a second endplate potential occurs before the first has reached its maximum then the second secretion will be masked and therefore not detected. Empirical treatments of this process have been attempted (Baldo *et al.* 1986) but a theoretical basis for this process is required. A cylindrical version of cable theory provides the theoretical model for this process.

(*a*) *Quantal secretion on a two-dimensional cable*

In their original description of the extracellularly recorded electrical signs of quantal secretion, del Castillo & Katz (1956) noted that 'the extracellular currents, therefore, converge from the large surrounding surface of the fibre into a highly localized region' so that one may consider 'an active spot equivalent to a small hole in a large sheet of insulating membrane'. At this level of spatial resolution, with the recording electrode localized to the active spot, current flow due to the action of the transmitter quantum must be considered as occurring initially in a two-dimensional sheet. This is in contrast to focal intracellular recording of the endplate potential in which the current flow can be described simply in terms of the spread of charge along a one-dimensional fibre (Fatt & Katz 1951). The following theory is then developed for the spread of charge applied instantaneously at a point on a cable of non-negligible diameter, so that current flows both transversely and along the length of the cylindrical cable. The theory is an extension of standard linear cable theory (Hodgkin & Rushton 1946; Tuckwell 1988). Only a deterministic version of cable theory will be used in these models. Incorporating random sources of variability in potential would considerably increase the level of mathematical analysis required, whereas the main use of cable theory here is to explain the detection-error problem, rather than to model accurately the electrical potential.

The potential at any point on the surface of the 'cylinder' will first be derived, based on the assumption that the current has been delivered as an instantaneous point charge. However, the actual miniature endplate current is not delivered as an instantaneous charge but rather as a (fast) time varying function. A commonly used model for this function is $I(t) = Q\alpha^2 t\,\mathrm{e}^{-\alpha t}$ (Jack *et al.* 1975; Tuckwell 1988), where $Q = \int_0^\infty I(t)\,\mathrm{d}t$ is the total charge delivered by the quantum and α is the rate constant. The potential resulting from the current function, $I(t)$, will then be obtained as the convolution of this current function with the potential resulting from the instantaneous charge (Green's function).

The length of neuron terminal will be approximated as a cylinder of infinite length. Define the coordinates of a point on the surface of the cylindrical fibre as $\boldsymbol{x} = (x_1, x_2)$ (mm), $-\infty < x_1 < \infty$; $-\pi r \leqslant x_2 \leqslant \pi r$, where r is the radius of the cylindrical cell (mm). Next, define the following electrical constants: r_e, extracellular resistance per unit length (Ω mm^{-1}); r_i, intracellular resistance per unit length (Ω mm^{-1}); r_m, membrane resistance multiplied by unit length (Ω mm); c_m, membrane capacitance per unit length (F mm^{-1}).

Also, define the following electrical variables: V_e, potential in the extracellular fluid (V); V_i, potential in the intracellular fluid (V); V_m, potential difference across cellular membrane (V); I_A, total current applied extracellularly (A).

All these quantities are functions of time t (ms) and location $\boldsymbol{x} = (x_1, x_2)$ (mm). The membrane potential $V_\mathrm{m} = V_\mathrm{m}(x_1, x_2, t)$ as a result of a unit charge delivered instantaneously at the origin $\boldsymbol{x} = (0, 0)$ at time $t = 0$ is given by

$$V_\mathrm{m}(x_1, x_2, t) = \frac{r_\mathrm{m} r_\mathrm{e}}{r_\mathrm{e}+r_\mathrm{i}} \exp\left(-\frac{t}{r_\mathrm{m} c_\mathrm{m}}\right) \times \left[\left(\frac{(r_\mathrm{e}+r_\mathrm{i})\, c_\mathrm{m}}{4\pi t}\right)^{\frac{1}{2}} \exp\left(-\frac{(r_\mathrm{e}+r_\mathrm{i})\, c_\mathrm{m}\, x_1^2}{4t}\right)\right] \times \left[\left(\frac{(r_\mathrm{e}+r_\mathrm{i})\, c_\mathrm{m}}{4\pi t}\right)^{\frac{1}{2}} \sum_{k=-\infty}^{\infty} \exp\left(-\frac{(r_\mathrm{e}+r_\mathrm{i})\, c_\mathrm{m}(x_2 - 2\pi r k)^2}{4t}\right)\right], \tag{5}$$

(see appendix A*a* for proof). The solution can be considered as being the product of three components: an attenuation component, a gaussian component along the length of the cylinder and a 'wrapped' gaussian component around the circumference of the cylinder.

However, it is not the potential difference across the membrane that is recorded, but the extracellular potential, in the present situation. In general, the relation between the potentials is given by $V_\mathrm{m} = V_\mathrm{e} - V_\mathrm{i}$, but in the 'extrapolar region' (away from where the current charge was delivered), $V_\mathrm{m} = [(r_\mathrm{e}+r_\mathrm{i})/r_\mathrm{e}]\ V_\mathrm{e}$ (see Hodgkin & Rushton 1946). So V_e can be calculated as

$$V_\mathrm{e} = r_\mathrm{e}/(r_\mathrm{e}+r_\mathrm{i})\ V_\mathrm{m}.$$

It is now assumed that, if a quantum is released, it will be received at the nearest point on the 'cylinder' that is along the line $x_2 = 0$. By writing y for x_1 and setting x_2 to zero, the Green's function for a point release at the origin is obtained from (5) as

$$G(y, t) = r_\mathrm{m}\left(\frac{r_\mathrm{e}}{r_\mathrm{e}+r_\mathrm{i}}\right)^2 \left(\frac{(r_\mathrm{e}+r_\mathrm{i})\, c_\mathrm{m}}{4\pi t}\right) \times \exp\left(-\frac{t}{r_\mathrm{m} c_\mathrm{m}} - \frac{(r_\mathrm{e}+r_\mathrm{i})\, c_m y^2}{4t}\right) \times \left[1 + 2\sum_{k=1}^{\infty} \exp\left(-\frac{(r_\mathrm{e}+r_\mathrm{i})\, c_\mathrm{m}(2\pi r k)^2}{4t}\right)\right].$$

PHILOSOPHICAL TRANSACTIONS OF THE ROYAL SOCIETY B BIOLOGICAL SCIENCES

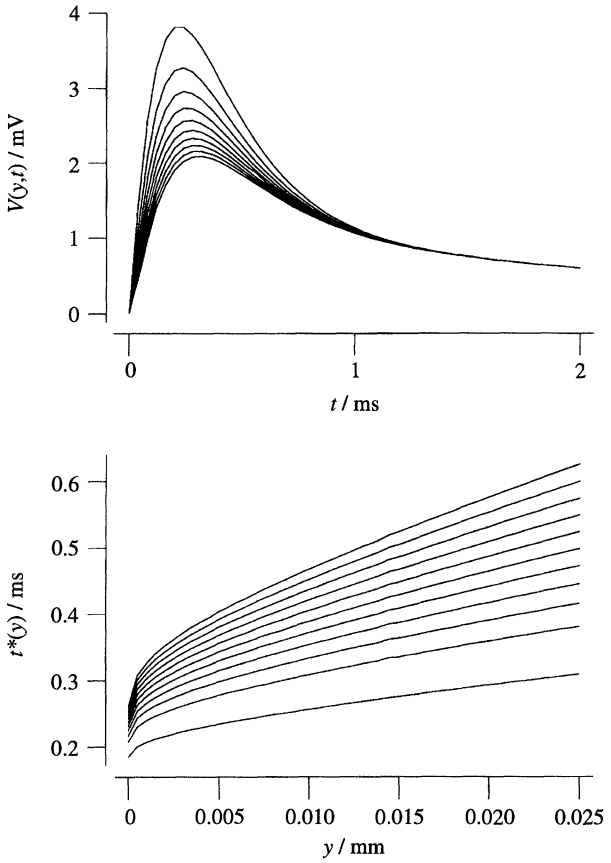

Figure 4. The potential based on a two-dimensional (cylindrical) cable model, due to injection of current at a point according to $I(t) = Q\alpha^2 t\,e^{-\alpha t}$. The upper figure shows the time course of the potential $V(y,t)$ at varying longitudinal distances between the recording electrode and point of injection, $y(\alpha = 6.25\ \mathrm{ms}^{-1}$ in all traces). The curves are for releases at $y = 0.0025, 0.0050, \ldots, 0.025$ mm, with the release at 0.0025 mm being the top curve. The lower figure shows the time to reach maximum potential and decline by an amount Δ_V, $t^*(y)$, as a function of this distance. These curves are shown for different values of the decline amount, $\Delta_V = 0$, 0.0005, …, 0.005 mV, with no decline, $\Delta_V = 0$ mV, being the bottom curve.

Next, the extracellular potential can be calculated from the convolution of $I(t)$ with $G(y,t)$ (see appendix A*b* for details). For simplicity, the subscript e will be dropped from the V_e. That is,

$$V(y,t) = \int_0^t G(y, t-s)\, I(s)\, \mathrm{d}s.$$

Qualitatively, the time trace of $V(y,t)$ is similar to that of $I(t)$ but takes longer to reach its maximum (after $t = \alpha^{-1}$). Further, this maximum occurs later and the value declines as $|y|$ increases (figure 4). For the detection process, the following numerical functions are defined. Firstly, let $t(y)$ be the time to reach its peak potential, for a quantal secretion at distance y away from the recording electrode. Secondly, let $t^*(y)$ be the time required (for a quantum at distance y) for the potential measured at the origin to have reached peak potential and then declined by an amount Δ_V. The earliest that a second quantum could be detected is at time $t^*(y)$ after the first release (at distance y) has begun.

Examples of $t^*(y)$ curves are shown in figure 4. As well as $t^*(y)$ increasing monotonically with y, it is seen that increasing the amount Δ_V increases the amount of time required to drop to this level.

In addition, the inverse of the function $t^*(y)$ is also required, labelled $y^*(t)$. It is the distance y at which the potential is maximized and declined by an amount Δ_V as a function of time t. That is, it is the location of a (first) quantal release that will just allow a release occurring at time t later to be detected.

(*b*) *Detection of multiple quantal secretions on a two-dimensional cable*

The next point to consider is the probabilistic model for detection. As quantal secretion was confined to a small length of a single terminal branch, by localizing calcium to this length, this secretion is assumed to occur within a spatial corridor of length $\pm\Delta_y$. The probability of secretion from a release site Y within $\pm\Delta_y$ will be taken as being uniform; that is, Y is a uniform random variable on $[-\Delta_y, +\Delta_y]$ and $|Y|$ is uniform on $[0, \Delta_y]$.

As before let $s_1 = t_2 - t_1$ be the time interval between the first and second release and let y_1 be the location of the first release. Let $\mathscr{D}$ be the event that the second release is detectable; that is, the second release occurs after the first reaches its maximum potential, and declined by Δ_V. Then,

$$P(\mathscr{D} \mid s_1, y_1) = \begin{cases} 1 & s_1 > t^*(y_1) \\ 0 & 0 \leqslant s_1 \leqslant t^*(y_1) \end{cases} = \begin{cases} 1 & |y_1| < y^*(s_1) \\ 0 & y^*(s_1) \leqslant |y_1| \leqslant \Delta_y. \end{cases}$$

So for a second quantal release, detection depends on both the interval between quantal releases and the location of the first quantal release. That is, increasing elapsed time (s_1) increases the probability that the second quantal release will be detected; similarly, more distant first quantal releases (large y_1) reduce the probability of a second release being detected, owing to the altered shape of the potential function as predicted from the cable equations.

Next, the probability that the second release will be detected given that it occurs at time s_1 after the first release is

$$P(\mathscr{D} \mid s_1) = \int_{-\Delta_y}^{+\Delta_y} \frac{1}{2\Delta_y} P(\mathscr{D} \mid s_1, y_1)\, \mathrm{d}y_1 = \begin{cases} 1 & s_1 > t^*(\Delta_y) \\ (1/\Delta_y)\, y^*(s_1) & t^*(0) \leqslant s_1 \leqslant t^*(\Delta_y) \\ 0 & 0 \leqslant s_1 \leqslant t^*(0). \end{cases}$$

With an asterisk indicating joint distributions with $\mathscr{D}$, the improper densities and probabilities of no release are as follows. The conditional probability density function of T_2 given $T_1 = t_1$ is

$$f^*_{T_2}(t_2 \mid t_1) = f_{T_2}(t_2 \mid t_1)\, P(\mathscr{D} \mid t_2 - t_1), \quad t_2 > t_1 + t^*(0) \qquad (6)$$

and the conditional probability of no finite T_2 is

$$P^*(T_2 = \infty \mid T_1 = t_1) = 1 - \int_{t_1 + t^*(0)}^{\infty} f_{T_2}(t_2 \mid t_1)\, P(\mathscr{D} \mid t_2 - t_1)\, \mathrm{d}t_2. \qquad (7)$$

PHILOSOPHICAL TRANSACTIONS OF THE ROYAL SOCIETY B BIOLOGICAL SCIENCES

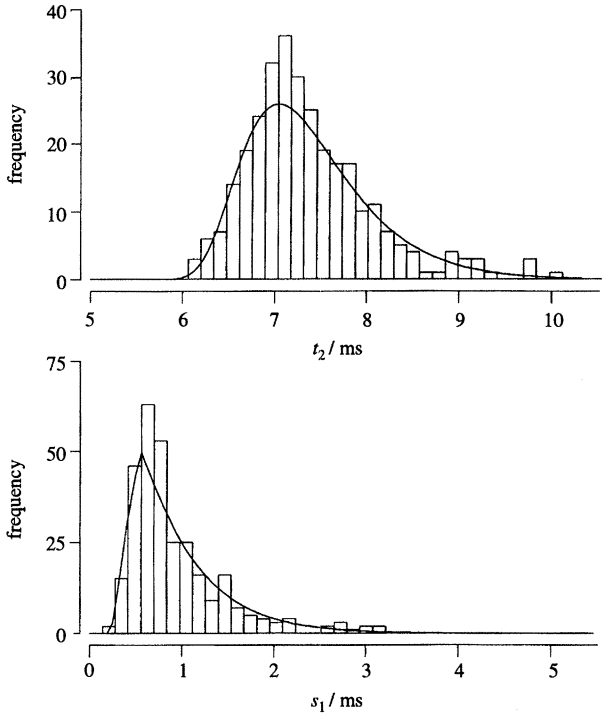

Figure 5. Comparison of the observed times of quantal secretions (histogram) with that of the predicted distribution (solid line) according to the fusion-pore model with detection-error correction. Times are for the second quantal secretion (t_2) and the interval between first and second quantal secretions ($s_1 = t_2 - t_1$). Estimates of the parameters in the model were obtained from the first and second quantal secretion times in experiment 1 ($\hat{\lambda} = 3.38$ ms^{-1}, $\hat{\gamma} = 2.91$ ms, $\hat{\tau} = 5.33$ ms and $\hat{\Delta}_V = 0.00232$ mV.

The joint probability density function of (T_1, T_2) is

$$f^*_T(t_1, t_2) = f_{T_1}(t_1) f_{T_2}(t_2 | t_1)\, P(\mathscr{D} | t_2 - t_1), t_2 > t_1, t_1 > 0$$

and from this the marginal probability density function of T_2 is obtained as

$$f^*_{T_2}(t_2) = \int_0^{t_2 - t^*(0)} f_{T_1}(t_1) f_{T_2}(t_2 | t_1)\, P(\mathscr{D} | t_2 - t_1)\, \mathrm{d}t_1, \qquad t_2 > t^*(0).$$

The probability density function of $S_1 = T_2 - T_1$ is now

$$f^*_{S_1}(s_1) = f_{S_1}(s_1)\, P(\mathscr{D} | s_1), \quad s_1 > t^*(0).$$

(*c*) *Success of the fusion-pore model with allowance for detection errors in predicting second quantal latencies*

The detection error model was fitted to the same data set described in §3*a*. For the reasons given there, k was set at five. The following electrical constants for the cable theory were taken from Hodgkin & Nakajima (1972, set 2): $r = 0.04$ mm, $r_i = 3.37 \times 10^5\ \Omega\ \mathrm{mm}^{-1}$, $r_m = 1.22 \times 10^6\ \Omega$ mm, $c_m = 1.56 \times 10^{-8}$ F mm^{-1}. From Hodgkin & Rushton (1946), $r_e = 0.81 \times r_i\ \Omega\ \mathrm{mm}^{-1}$ based on the average of 13 experiments; so $r_e = 2.73 \times 10^5\ \Omega\ \mathrm{mm}^{-1}$. The total quantal charge is taken as 10^{-11} C, and the window width for quantal detection is taken as $\Delta_y = 0.025$ mm. Based on the likelihood surface, it is evident that the parameter estimates for α and Δ_V are highly positively correlated. Consequently, α was set at 6.25 ms^{-1}, based on quantal current data in Gage & Armstrong (1968).

By using the estimates obtained in §3*a* for λ, γ and τ, Δ_V was estimated by maximum likelihood as 0.00232 mV. Full likelihood produced negligible changes to estimates ($\hat{\lambda} = 3.38$ ms^{-1}, $\hat{\gamma} = 2.91$ ms^{-1}, $\hat{\tau} = 5.33$ ms, and $\hat{\Delta}_V = 0.00232$ mV).

The fitted distributions and histograms of the first experiment, based on the estimates of λ, γ, τ and Δ_V, are shown in figure 5. The fit of the time till the second quantal secretion is now much improved, although the model does not predict the extreme peak of the density. The fit to s_1 is also much improved.

5. THE FUSION-PORE MODEL WITH AUTOINHIBITION AND ALLOWANCE FOR ERRORS IN DETECTION IN MULTIPLE QUANTAL SECRETIONS: THE COMBINED MODEL

Good predictions of all the latency–frequency distributions for second and later quanta were obtained once allowance was made for errors in detection. However, it is still possible that the predictions could be improved if a scheme that incorporates the autoinhibition of quantal secretion by previously secreted quanta within the period of increased probability of secretion following a nerve impulse. For example, detection errors may result in early second quantal secretions not being seen, and inhibition may result in late second quantal secretions not occurring. To see if this is the case, an autoinhibitory model is first developed (§5*a*) and this is combined with the detection error model to give a combined model (§5*b*). This is then used to test if a finite autoinhibitory mechanism can be detected (§5*c*).

(*a*) *The autoinhibitory model*

Bennett & Robinson (1990) described a theory of autoinhibition whereby later quantal secretions would be impeded by earlier ones. Figure 6 shows the interaction between release sites resulting in autoinhibition. The ordinate shows the position of the release site $[0, 1]$, and the abscissa the time of release $[0, \infty]$. Sites that secrete a quantum of neurotransmitter also initiate an inhibitory process. This inhibitory influence spreads at a linear rate v so that any point within the 'cone' will be prevented from releasing neurotransmitter.

The probability distributions for release times for the autoinhibition model will now be outlined. The distribution of the time till first secretion, T_1, will be as defined for the fusion-pore model. With the first quantal secretion at (x_1, t_1), define the indicator variable for the inhibition of a secretion at (x_2, t_2),

$$I_\phi(x_1, x_2, t_1, t_2) = \begin{cases} 1 & \text{if } (x_2, t_2) \text{ is in the area free from inhibition} \\ 0 & \text{otherwise} \end{cases}$$

PHILOSOPHICAL TRANSACTIONS OF THE ROYAL SOCIETY B BIOLOGICAL SCIENCES

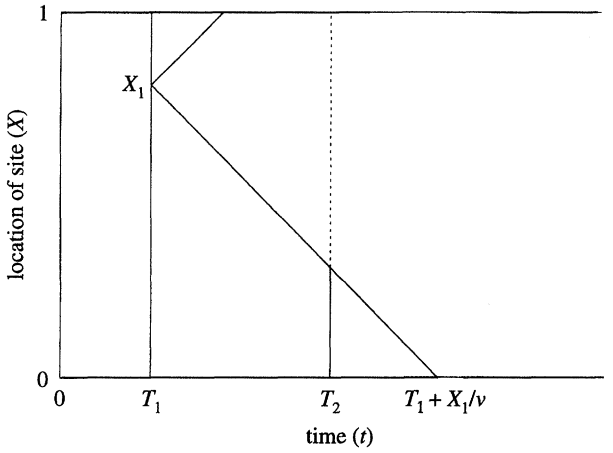

Figure 6. Graphical representation of the model of inhibition. The first quantal secretion is at (X_1, T_1), and an inhibitor spreads out linearly in both directions at rate v. A release at time T_2 would be locked if it were located on the broken line; otherwise it would release and also produce an inhibitory spreading 'cone'. No releases are possible after time T_1+X_1/v.

and let

$$\phi(x_1,t_1,t_2)=\int_0^1 I_\phi(x_1,x_2,t_1,t_2)\,\mathrm{d}x_2$$
$$=\max[x_1-v(t_2-t_1),0]$$
$$+\max[1-x_1-v(t_2-t_1),0],\ 0\leqslant x_1\leqslant 1;\ t_2>t_1.$$

Also define the cumulative rate function,

$$\Lambda_\phi(t_2\,|\,x_1,t_1)=\int_{t_1}^{t_2}\lambda(u_2)\,\phi(x_1,t_1,u_2)\,\mathrm{d}u_2,$$

and instantaneous rate function,

$$\lambda_\phi(t_2\,|\,x_1,t_1)=\mathrm{d}[\Lambda_\phi(t_2,|\,x_1,t_1)]/\mathrm{d}t_2.$$

A subscript ϕ will be used here to indicate the autoinhibition model as opposed to the basic fusion-pore model and detection-error model. The conditional probability density function of T_2 given $T_1=t_1$ is

$$f_{\phi T_2}(t_2\,|\,t_1)=\int_0^1\lambda_\phi(t_2\,|\,x_1,t_1)\exp[-\Lambda_\phi(t_2\,|\,x_1,t_1)]\,\mathrm{d}x_1,$$
$$t_1<t_2<t_1+1/v.$$

The probability of no further releases after time t_1 is obtained by observing that no further releases can occur after time t_1+1/v, that is,

$$P_\phi(T_2=\infty\,|\,T_1=t_1)=\int_0^1\exp\left[-\Lambda_\phi\left(t_1+\frac{1}{v}\,\middle|\,x_1,t_1\right)\right]\mathrm{d}x_1.$$

The joint density of (T_1, T_2) can be calculated as

$$f_{\phi T}(t_1,t_2)=f_{T_1}(t_1)f_{\phi T_2}(t_2\,|\,t_1),\quad t_1<t_2<t_1+1/v,t_1>0,$$

and the marginal probability density function of T_2 is

$$f_{\phi T_2}(t_2)=\int_{\max(t_2-1/v,\,0)}^{t_2}f_{\phi T}(t_1,t_2)\,\mathrm{d}t_1,\quad t_2>0.$$

Also of interest is the distribution of the time interval between successive releases, $S_1=T_2-T_1$, and this has probability density function

$$f_{\phi S_1}(s_1)=\int_0^\infty f_{\phi T}(t_1,s_1+t_1)\,\mathrm{d}t_1,\quad 0<s_1<\frac{1}{v}.$$

Note that this autoinhibitory model considers the Poisson limit as the number of release sites, n, tends to infinity and the calcium ion binding rate, $\alpha(x_i)$, tends to zero (and the probability of release tends to zero). Consequently, the probability that any one site would release more than one quantum is vanishingly small, regardless of the value of v. So, under this model, it is not appropriate to consider a situation of auto-inhibition within a *single* release site. However, in a model with a finite (small) number of sites, this situation could be considered.

(*b*) *The combined model*

Calculation of density and probability expressions for the release times follows in the same manner as for the detection error model; so relatively little new material needs to be derived. Essentially, these expressions are obtained by using the inhibition model terms, $f_{\phi S_1}(s_1)$ and $f_{\phi T_2}(t_2\,|\,t_1)$ in place of the basic model terms, $f_{S_1}(s_1)$ and $f_{T_2}(t_2\,|\,t_1)$, and substituting these in the expressions for the detection error model.

With the * and ϕ notation to indicate joint distributions with $\mathscr{D}$, and with inhibition, the following expressions are obtained. The probability density function for the second release, given the time of the first release, is

$$f^*_{\phi T_2}(t_2\,|\,t_1)=f_{\phi T_2}(t_2\,|\,t_1)\,P(\mathscr{D}\,|\,t_2-t_1),$$
$$t_1+t^*(0)<t_2<t_1+1/v,\quad (8)$$

and the probability of no (finite) second release, given the time of the first release, is

$$P^*_\phi(T_2=\infty\,|\,T_1-t_1)$$
$$=1-\int_{t_1+t^*(0)}^{t_1+1/v}f_{\phi T_2}(t_2\,|\,t_1)\,P(\mathscr{D}\,|\,t_2-t_1)\,\mathrm{d}t_2.\quad (9)$$

The joint probability density function of (T_1, T_2) is

$$f^*_{\phi T}(t_1,t_2)=f_{T_1(t_1)}f_\phi T_2(t_2\,|\,t_1)\,P(\mathscr{D}\,|\,t_2-t_1),$$
$$t_2>t_1+t^*(0),t_1>0,$$

and from this the marginal probability density function of T_2 is

$$f^*_{\phi T_2}(t_2)=\int_{\max[t_2-1/v,\,0]}^{t_2-t^*(0)}f_{T_1}(t_1)f_{\phi T_2}(t_2\,|\,t_1)\,P(\mathscr{D}\,|\,t_2-t_1)\,\mathrm{d}t_1,$$
$$t_2>t^*(0).$$

The probability density function of the inter-release times, $S_1=T_2-T_1$, is

$$f^*_{\phi S_1}(s_1)=f_{\phi S_1}(s_1)\,P(\mathscr{D}\,|\,s_1),\quad t^*(0)<s_1<1/v.$$

(*c*) *The combined model estimates autoinhibition as zero*

With use of the estimates of the main time course parameters (λ, γ, k and τ) obtained in §3*a*, together with the detection error parameter (Δ_V) given in §4*c*, the likelihood of the data was maximized to estimate v. For the first experiment this gave $\hat{v}=0$ mm s^{-1}, indicating no detectable autoinhibition. Full likelihood maximization of all parameters returned the same

PHILOSOPHICAL TRANSACTIONS OF THE ROYAL SOCIETY B BIOLOGICAL SCIENCES

Table 2. *Parametric bootstrap of the parameter estimates for the experimental data*

(Bootstrap values based on 200 simulations for estimation of (λ, γ, τ, Δ_V) and ten simulations for estimation of (λ, γ, τ, Δ_V, v).)

parameter	estimate	bootstrap mean	bootstrap s.e.	bootstrap 95% c.i.
λ (ms^{-1})	3.39	3.39	0.0866	3.24–3.54
γ (ms^{-1})	2.91	2.92	0.789	2.78–3.05
τ (ms)	5.33	5.33	0.262	5.29–5.37
Δ_V (mV)	0.00232	0.00231	0.000370	0.00170–0.00293
v (mm s^{-1})	0	1.5	1.5	—

Table 3. *Descriptive statistics for the first four releases* (t_i; $i = 1, \ldots, 4$) *and intervals between releases* ($s_i = t_{i+1} - t_i$; $i = 1, \ldots, 3$)

(Comparison with a Monte Carlo evaluation of 10000 simulations. Units of time are milliseconds.)

	mean		s.d.	
	data	simulation	data	simulation
t_1	6.626	6.642	0.575	0.623
t_2	7.354	7.442	0.683	0.688
t_3	7.868	8.015	0.573	0.694
t_4	8.690	8.474	0.863	0.651
s_1	0.932	1.034	0.530	0.563
s_2	0.960	0.978	0.437	0.540
s_3	1.008	0.932	0.647	0.483

Table 4. *Frequency distribution for the number of quantal secretions*

(Comparison with a Monte Carlo evaluation of 10000 simulations.)

number of secretions	frequency	relative frequency	
		data	simulation
0	104	0.130	0.130
1	392	0.490	0.455
2	238	0.298	0.341
3	60	0.075	0.068
4+	6	0.008	0.006
mean		1.340	1.365
variance		0.680	0.664
ratio		1.970	2.056

estimates. Thus the fusion-pore model with detection errors is alone sufficient to model the data of the first experiment.

As a check on the accuracy of these parameter estimates, a small scale parametric bootstrap procedure has been done. The parametric bootstrap is useful when the underlying distribution can be assumed, but its properties (such as bias and standard errors of estimators) are too difficult or intractable to obtain analytically (Efron & Tibshirani 1986). Details of this procedure can be found in appendix C, but essentially it involves generation of data from the model with its parameter estimates to obtain a new set of estimates for each set. After sufficient sets have been obtained, the mean of the estimates can be used to assess bias, and the standard deviation taken as an empirical standard error of the original parameter estimate. Ideally, a large number of sets of data would be generated, but, owing to the computation required, estimation of λ, γ, τ and Δ_V was limited to 200 times, and v ten times.

For v, the ten estimates (in sorted order) were 0, 0, 0, 0, 0, 1.45, 1.70, 3.55, 3.60 and 4.20 mm s^{-1}), confirming that the amount of inhibition is small, if it occurs at all. For the other parameters, it is seen that there is negligible bias in their estimates (see table 2).

To examine the fit of the model, a Monte Carlo simulation ($N_{mc} = 10000$) was done with these parameter estimates. This will allow the model predictions for the third and fourth releases, as well as the first two, to be compared with the data. This is useful since none of the information in t_3 and t_4 was used in parameter estimation. Table 3 shows the times of releases, indicating good agreement for the t and the s. The frequency distribution of the number of releases is shown in table 4. A goodness of fit test shows no significant departure of the model from the data ($\chi^2 = 7.47$, d.f. = 4, $P = 0.113$). Note that the model also predicts the relatively small variance compared with the mean.

Since it is possible that the zero estimate of v in this data set (and others) might be due to a bias or inability to detect a non-zero value of v, an additional Monte Carlo study was done to assess the estimation of v. The inhibition parameter v was varied from 0 to 12.5 mm s^{-1} in steps of 2.5, with five replicates at each value of v. Even at $v = 2.5$ mm s^{-1} all five replicates gave non-zero values of $\hat{v}$ (with an average of 3.9 mm s^{-1}), which suggests that this method would detect inhibition, if it were present in the data.

6. ANALYSES OF OTHER DATA SETS

In addition to the main data set analysed here, twelve others have been provided, and all but the last four were for identical experimental conditions. The parameter estimates for the combined model are shown in table 5. The main feature is that in all data sets v was estimated as zero. In addition there is evidence that the main time course parameter estimates ($\hat{\lambda}$ and $\hat{\gamma}$) are positively correlated ($r = 0.93$), as was also suggested by the Monte Carlo study noted in §3*a*.

Also shown are the histograms and fitted distributions of these data sets (figure 7). All these graphs have been drawn to the same vertical and horizontal scales. In general the fit of the model to these sets of data is adequate. However, as with the first data set analysed, there are instances when the peaks in the histograms are not fully reproduced by the fitted distributions.

PHILOSOPHICAL TRANSACTIONS OF THE ROYAL SOCIETY B BIOLOGICAL SCIENCES

Table 5. *Parameter estimates for thirteen experimental data sets*

(The sample size for each data set is n (number of stimuli).)

data set	n	$\hat{v}$ mm s^{-1}	$\hat{\lambda}$ ms^{-1}	$\hat{\gamma}$ ms^{-1}	$\hat{\tau}$ ms	$\hat{\Delta}_v$ mV
1	800	0	3.38	2.91	5.33	0.002 32
2	198	0	2.49	2.21	4.64	0.003 71
3	196	0	3.28	2.86	4.87	0.002 71
4	800	0	1.59	1.54	4.14	0.003 11
5	400	0	3.73	2.86	3.32	0.002 68
6	400	0	3.78	2.93	3.44	0.007 89
7/8	800	0	2.72	2.13	3.55	0.008 21
9	800	0	3.49	2.86	3.79	0.008 99
10	800	0	2.41	2.11	3.15	0.005 45
F1	400	0	3.66	3.39	3.72	0.005 07
F2	400	0	3.49	3.47	3.98	0.004 34
F3	400	0	4.16	3.48	4.00	0.001 34
F4	400	0	4.23	3.42	3.97	0.001 91

7. DISCUSSION AND CONCLUSIONS

(*a*) *The probabilistic model of secretion*

The stochastic model used in the present work has been developed in terms of transmitter secretion consisting of three processes. Firstly calcium enters through voltage-sensitive calcium channels and then diffuses to the release site protein, a process that is taken as primarily responsible for the minimum synaptic delay (τ), estimated in the present case as 5.3 ms at about 3 °C. The mean open time of N-type calcium channels expected during a nerve impulse at this temperature is several milliseconds (Delcour *et al.* 1993), during which calcium diffuses from the open channel to reach a near peak concentration at the release-site protein (Yamada & Zucker 1992). The second process involves attachment of the calcium ions to k sites on the release protein and its subsequent conformational change, a procedure that has been taken as mostly responsible for the time course of the quantal secretion histograms, with the possibility that a bound calcium will become dissociated at rate γ determining the possible termination of the process; k was estimated as 5.40 and γ was 3.0 ms^{-1} for thirteen sets of release sites. There have been several different approaches to evaluating k, from about four in the early work of Dodge & Rahamimoff (1967), to five in the more recent research of Zucker & Fogelson (1986), and four in that of Augustine & Charlton (1986). The procedure for estimating k in the present work offers a value close to these. On the other hand there have not yet been investigations of the calcium binding protein kinetics, perhaps because synaptotagmin and GTPase Rab3a have only recently been recognized as the likely strategic calcium binding proteins in this process (Popov & Poo 1993; Johannes *et al.* 1994). Nevertheless the dissociation constant that terminates secretion has usually been given a value of about 1 ms^{-1} at 10 °C in other simulations of the secretory process, similar to the estimate in the present work for γ of 3.0 ms^{-1} (Yamada & Zucker 1992). Finally the question arises as to the time taken for the final step of exocytosis (rate constant δ above), which in some recent deterministic models has been taken as the rate limiting step in the secretory process (Parnas *et al.* 1989; Yamada & Zucker 1992). This has not been taken to be so in the present stochastic model, as δ is likely to be large (of the order of 10 ms^{-1}; Almers *et al.* 1989), even if the time course of exocytosis is determined by the 'stand alone flicker' of the fusion-pore (Neher 1993), in which transmitter is released through the pore without the vesicle undergoing complete fusion (Alvarez de Toledo *et al.* 1993). One caveat in the estimates of the parameters in the present model is that there are positive correlations between estimates of λ, γ and k, indicating that any particular value of one of these parameter estimates may not be considered in isolation from the others. Furthermore, the possibility that following quantal release a site becomes transiently refractory to further quantal release has not been considered in the model. Rather, the Poisson limit has been taken of a very low probability of release from a single site, so that the probability of two releases is negligibly small. The incorporation of a possible refractory state in future developments will require abandoning the Poisson limit.

(*b*) *Comparison with other models of secretion*

Deterministic models of the secretory process have been developed, based on various assumptions. Van der Kloot (1988*a*, *b*) suggested that there are three main elements in the process. The first involves calcium entry, its diffusion to the release-site protein with subsequent binding to the protein; this rate was taken to follow a gaussian form. Next, the release site protein undergoes a conformational change which occupies a relatively set time interval and is therefore responsible for the minimum synaptic delay of about 1.2 ms at 10 °C (Katz & Miledi 1965*b*). Finally, exocytosis occurs according to a first order process, with a time constant of 1.3 ms at 10 °C. This high Q_{10} of the synaptic delay (Katz & Miledi 1965*b*) is then attributed to the conformational change in the release-site protein. The influx of higher than normal levels of calcium ions into the terminal produced by exposure to 4-aminopyridine increases quantal output and increases the time-to-peak, without altering significantly the time course of decline of quantal secretion following an impulse (Van der Kloot 1988*b*). This observation is consistent with the Van der Kloot model in which the rising phase of the probability of secretion is mostly determined by the binding of calcium to the release-site protein with subsequent conformational change, whereas the declining phase of the probability is mostly limited by the time for exocytosis. Other deterministic models of secretion also divide the process into three steps, but regard the final step, namely exocytosis, as rate limiting and primarily responsible for the minimum synaptic delay (Parnas *et al.* 1989; Yamada & Zucker 1992). This emphasis arises as a consequence of considerations concerning the high temperature dependence of release being determined by the exocytotic process. The present model has also ascribed three discrete steps to the release process but

PHILOSOPHICAL TRANSACTIONS OF THE ROYAL SOCIETY B BIOLOGICAL SCIENCES

exocytosis has not been taken as rate limiting. Rather the binding of calcium ions and the subsequent conformation change in the release-site protein are primarily responsible for the early release period, which is more like the Van der Kloot (1988*b*) model, as argued in §7*a*. This conformational change may be the major temperature sensitive process in release (see also Yamada & Zucker 1992), rather than exocytosis (Monck & Fernández 1994). The present work shows that this model gives good predictions for the timing of third and fourth quantal delays (as well as the first two), with use of just the first two quantal delays to estimate the parameters of the model.

(*c*) *Binomial statistics of secretion and autoinhibition*

Quantal secretions from the entire motor-nerve terminal deviate from the predictions based on an underlying Poisson process, more closely following that of a binomial process (Wernig 1975; Bennett *et al.* 1975; Bennett & Fisher 1977; Bennett & Robinson 1990; compare with Wernig 1972*a*, *b* and Zucker 1973). One possible explanation offered is that following quantal secretion at a site, an autoinhibitory influence propagates from there to prevent secretion at adjacent sites thus decreasing the variance of quantal secretion from the terminal (Bennett & Robinson 1990).

Such a mechanism would also provide an explanation for the experimental observations on the effects of calcium ions on the binomial parameters n and p describing quantal secretion from the whole terminal as well as the relative constancy of p during facilitation and depression of quantal secretion (Bennett & Robinson 1990). In the present work, an analytical procedure has been introduced for determining the probability that a second quantal secretion will be detected given that it occurs at a specified time after the first secretion. This procedure, together with the stochastic model of the secretory process, gave a satisfactory prediction for the mean times for secretion (and standard deviations) involving third and fourth quanta, when the parameter estimates were determined from the first two quantal latencies. Combination of this approach with the model for autoinhibition, in which an inhibitory influence propagates from the site of quantal secretion at constant velocity, did not improve the predictions. There was therefore no evidence for an autoinhibitory mechanism, even though high quantal secretions were reached from a localized region of the terminal when using recording electrodes with high concentrations of calcium in a calcium-free bathing solution. It has been pointed out that claims regarding a lack of intra-trial autoinhibition, based on comparisons between λ_2 and λ_1 (Baldo *et al.* 1986), may not be accurate because of the relative insensitivity of this comparison (Bennett & Robinson 1990). However the present work shows that even later occurring quanta show independence, so that there is no evidence for autoinhibition. Therefore another mechanism must be sought to account for the binomial-like behaviour of quantal secretion from the entire motor-nerve terminal.

APPENDIX A. ELECTRICAL POTENTIAL THEORY

(*a*) *Derivation of the cable equation for the surface of a cylinder*

The membrane potential $V_m = V_m(x_1, x_2, t)$ as a result of a current I_A delivered extracellularly can be described by the partial differential equation,

$$\frac{r_m}{r_e + r_i}\left(\frac{\partial^2 V_m}{\partial x_1^2} + \frac{\partial^2 V_m}{\partial x_2^2}\right) - V_m = r_m c_m \frac{\partial V_m}{\partial t} - \frac{r_m r_e}{r_e + r_i} I_A, \qquad (10)$$

where r_e, r_i, r_m and c_m are the electrical constants as defined in §4*a*. This is seen as an extension of equation (2.0) of Hodgkin & Ruchton (1946), which considered the x_1 (longitudinal) dimension only.

The solution to this partial differential equation will be derived. The 'wrapping' constraint is

$$V_m(x_1, -\pi t, t) = V_m(x_1, \pi r, t), \quad t > 0.$$

Assume that I_A is a unit charge (1 C) delivered instantaneously at the origin $\boldsymbol{x} = (0, 0)$ at time $t = 0$. So the initial condition is

$$\lim_{t \to 0} V(x_1, x_2, t) = \delta(x_1)\,\delta(x_2)\frac{r_m r_e}{r_e + r_i}$$

where $\delta(\cdot)$ is the Dirac delta function.

Write V_m as a Fourier series in x_2,

$$V_m(x_1, x_2, t) = \tfrac{1}{2}F_0(x_1, t) + \sum_{k=1}^{\infty} F_k(x_1, t)\cos\left(\frac{k x_2}{r}\right).$$

By expanding equation (10) and equating Fourier coefficients,

$$\frac{r_m}{r_e + r_i}\frac{\partial^2 F_k}{\partial x_1^2} - \left(\frac{r_m}{r_e + r_i}\frac{k^2}{r^2} + 1\right)F_k = r_m c_m \frac{\partial F_k}{\partial t}, \quad k = 0, 1, 2, \ldots. \qquad (11)$$

The Fourier transform in x_1 of $F_k(x_1, t)$ is

$$\mathscr{F}_k(\omega, t) = \frac{1}{\sqrt{2\pi}}\int_{-\infty}^{\infty} F_k(x_1, t)\, e^{i\omega t}\, dx_1,$$

where $i = \sqrt{-1}$. So by taking Fourier transforms of x_1 of (11)

$$-\left(\frac{r_m}{r_e + r_i}\omega^2 + \frac{r_m}{r_e + r_i}\frac{k^2}{r_i r^2} + 1\right)\mathscr{F}_k = r_m c_m \frac{\partial \mathscr{F}_k}{\partial t}, \quad k = 0, 1, 2, \ldots$$

and the solution of this is

$$\mathscr{F}_k(\omega, t) = c_k \exp\left[-\frac{1}{r_m c_m}\left(\frac{r_m}{r_e + r_i}\omega^2 + \frac{r_m}{r_e + r_i}\frac{k^2}{r^2} + 1\right)t\right], \quad k = 0, 1, 2, \ldots.$$

PHILOSOPHICAL TRANSACTIONS OF THE ROYAL SOCIETY B BIOLOGICAL SCIENCES

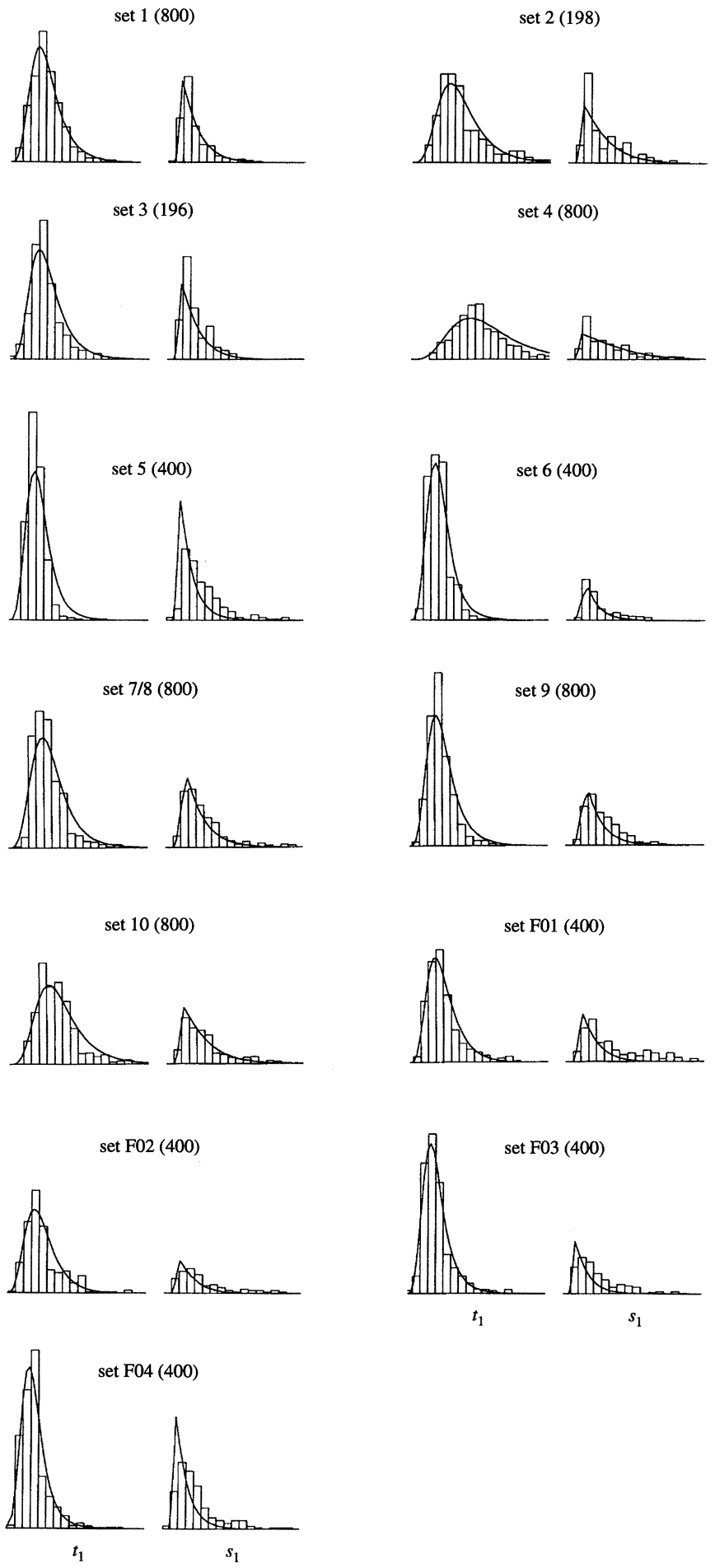

Figure 7. For description see opposite.

PHILOSOPHICAL TRANSACTIONS OF THE ROYAL SOCIETY B BIOLOGICAL SCIENCES

A Fourier series in x_2 for the initial condition gives

$$\lim_{t\to 0}\left[\tfrac{1}{2}F_0(x_1,t)+\sum_{k=1}^{\infty}F_k(x_1,t)\cos\left(\frac{kx_2}{r}\right)\right]$$
$$=\frac{r_m r_e}{r_e+r_i}\delta(x_1)\left[\tfrac{1}{2}\Delta_0+\sum_{k=1}^{\infty}\Delta_k\cos\left(\frac{kx_2}{r}\right)\right],$$

where $\Delta_k = 1/\pi r$, $k = 0, 1, 2, \ldots$. Hence,

$$\lim_{t\to 0}F_k(x_1,t)=\frac{r_m r_e}{r_e+r_i}\frac{1}{\pi r}\delta(x_1),\quad k=0,1,2,\ldots.$$

So the Fourier transform in x_1 for the initial condition is

$$\mathscr{F}_k(\omega,0)=\frac{1}{\sqrt{2\pi}}\frac{r_m r_e}{r_e+r_i}\frac{1}{\pi r},\quad k=0,1,2,\ldots,$$

and

$$c_k=\frac{1}{\sqrt{2\pi}}\frac{r_m r_e}{r_e+r_i}\frac{1}{\pi r}.$$

Therefore,

$$\mathscr{F}_k(\omega,t)=\frac{1}{\sqrt{2\pi}}\frac{r_m r_e}{r_e+r_i}\frac{1}{\pi r}$$
$$\times\exp\left[-\frac{1}{r_m c_m}\left(\frac{r_m}{r_e+r_i}\omega^2+\frac{r_m}{r_e+r_i}\frac{k^2}{r^2}+1\right)t\right],$$
$$k=0,1,2,\ldots.$$

Take the inverse Fourier transform,

$$F_k(x_1,t)=\sqrt{\left(\frac{(r_e+r_i)c_m}{4\pi t}\right)}\frac{r_m r_e}{r_e+r_i}\frac{1}{\pi r}$$
$$\times\exp\left[-\frac{1}{r_m c_m}\left(\frac{r_m}{r_e+r_i}\frac{k^2}{r^2}+1\right)t-\frac{(r_e+r_i)c_m x_1^2}{4t}\right].$$

Substitution of these Fourier coefficients into (11) gives

$$V_m(x_1,x_2,t)=\frac{r_m r_e}{r_e+r_i}\exp\left(-\frac{t}{r_m c_m}\right)$$
$$\times\left[\sqrt{\left(\frac{(r_e+r_i)c_m}{4\pi t}\right)}\exp\left(-\frac{(r_e+r_i)c_m x_1^2}{4t}\right)\right]$$
$$\times\left[\frac{1}{2\pi r}+\frac{1}{\pi r}\sum_{k=1}^{\infty}\exp\left(-\frac{k^2t/r^2}{(r_e+r_i)c_m}\right)\cos\left(\frac{kx_2}{r}\right)\right]\quad(12)$$
$$=\frac{r_m r_e}{r_e+r_i}\exp\left(-\frac{t}{r_m c_m}\right)$$
$$\times\left[\sqrt{\left(\frac{(r_e+r_i)c_m}{4\pi t}\right)}\exp\left(-\frac{(r_e+r_i)c_m x_1^2}{4t}\right)\right]$$
$$\times\left[\sqrt{\left(\frac{(r_e+r_i)c_m}{4\pi t}\right)}\right.$$
$$\left.\times\sum_{j=-\infty}^{\infty}\exp\left(-\frac{(r_e+r_i)c_m(x_2-2\pi rj)^2}{4t}\right)\right].\quad(13)$$

The alternative series expansion for the potential (13) is based on the method of Stephens (1963). Let

$$g(x_2)$$
$$=\sqrt{\left(\frac{(r_e+r_i)c_m}{4\pi t}\right)}\sum_{j=-\infty}^{\infty}\exp\left(-\frac{(r_e+r_i)c_m(x_2-2\pi rj)^2}{4t}\right).$$

This may be written as a Fourier series expansion,

$$g(x_2)=\tfrac{1}{2}G_0(t)+\sum_{k=1}^{\infty}G_k(t)\cos\left(\frac{kx_2}{r}\right)$$

since $g(\cdot)$ is an even function. The Fourier coefficients are obtained as

$$G_k(t)=\frac{1}{\pi r}\exp\left(-\frac{k^2t/r^2}{(r_e+r_i)c_m}\right),\quad k=0,1,2,\ldots.$$

Substitution of these Fourier coefficients gives

$$g(x_2)=\frac{1}{2\pi r}+\frac{1}{\pi r}\sum_{k=1}^{\infty}\exp\left(-\frac{k^2t/r^2}{(r_e+r_i)c_m}\right)\cos\left(\frac{kx_2}{r}\right)$$

as required.

Note that the second form of the solution of the partial differential equation (13) is suited to calculation of small times as considered in the present application, that is, when there has not been sufficient time for the potential to wrap many times around the cylinder. For larger times, the first form of the expression (12) converges more quickly corresponding to a nearly 'uniform' situation where the potential is nearly equal around the circumference of the cylinder.

(*b*) *Derivation of the membrane potential and related numerical functions, for the cylinder cable equation model*

(i) *Membrane potential*

The membrane potential as a result of a quantal charge is derived here. It is obtained as the convolution of the Green's function, $G(y,t)$, with the current function, $I(t)$,

$$V(y,t)=\int_0^t G(y,t-s)\,I(s)\,\mathrm{d}s.$$

The current function takes the α form,

$$I(t)=Q\alpha^2 t\,\mathrm{e}^{-\alpha t},$$

where Q is the total charge delivered by the quantum, and α is the rate constant. Expressions for $V(y,t)$ will be derived based on two equivalent Green's functions.

By using (12) and letting $x_1 = y$ and $x_2 = 0$ Green's function 1 is obtained,

$$G_1(y,t)=r_m\left(\frac{r_e}{r_e+r_i}\right)^2\sqrt{\left(\frac{(r_e+r_i)c_m}{4\pi t}\right)}$$
$$\times\exp\left(-\frac{t}{r_m c_m}-\frac{(r_e+r_i)c_m y^2}{4t}\right)$$
$$\times\left[\frac{1}{2\pi r}+\frac{1}{\pi r}\sum_{k=1}^{\infty}\exp\left(-\frac{k^2t/r^2}{(r_e+r_i)c_m}\right)\right].$$

Figure 7. Distribution of T_1 and $S_1 = T_2 - T_1$ of thirteen data sets for the combined model. Histograms are shown along with the fitted densities based on the parameter estimates. The length of abscissa is 5 ms on all graphs (with a bin size of 0.14 ms), and the origin for the t_1 distributions has been set at the estimated value of τ. All the vertical scales are also on the same scale, such that the areas under the curve represent the probability of obtaining a finite t_1 or finite s_1.

PHILOSOPHICAL TRANSACTIONS OF THE ROYAL SOCIETY B BIOLOGICAL SCIENCES

Define

$$C = r_m\left(\frac{r_e}{r_e+r_i}\right)^2 Q\alpha^2$$

and

$$J(t;\eta,\xi,\nu) = \int_0^t \exp\left(-\eta u - \frac{\xi}{u}\right) u^\nu \, du.$$

Then

$$V(y,t) = \frac{C}{\pi r}\sqrt{\left(\frac{(r_e+r_i)\,c_m}{4\pi}\right)} e^{-\alpha t} \times\left\{\tfrac{1}{2}[tJ(t;\eta_0,\xi,-\tfrac{1}{2}) - J(t;\eta_0,\xi,\tfrac{1}{2})] + \sum_{k=1}^{\infty}[tJ(t;\eta_k,\xi,-\tfrac{1}{2}) - J(t;\eta_k,\xi,\tfrac{1}{2})]\right\},$$

where

$$\eta_k = \frac{1}{r_m c_m} - \alpha + \frac{k^2/r^2}{(r_e+r_i)\,c_m}, \quad k = 0, 1, \ldots,$$

$$\xi = \tfrac{1}{4}[(r_e+r_i)\,c_m y^2].$$

Alternatively, by using (13) and letting $x_1 = y$ and $x_2 = 0$ Green's function 2 is obtained,

$$G_2(y,t) = r_m\left(\frac{r_e}{r_e+r_i}\right)^2\left(\frac{(r_e+r_i)\,c_m}{4\pi t}\right) \times \exp\left(-\frac{t}{r_m c_m} - \frac{(r_e+r_i)\,c_m y^2}{4t}\right) \times\left[1 + 2\sum_{k=1}^{\infty}\exp\left(-\frac{(r_e+r_i)\,c_m(2\pi r k)^2}{4t}\right)\right],$$

where $G_1(y,t) = G_2(y,t)$. So

$$V(y,t) = \frac{C(r_e+r_i)c_m}{4\pi} e^{-\alpha t} \times\left\{\tfrac{1}{2}[tJ(t;\eta,\xi_0,-1) - J(t;\eta,\xi_0,0)] + \sum_{k=1}^{\infty}[tJ(t;\eta,\xi_k,-1) - J(t;\eta,\xi_k,0)]\right\},$$

where

$$\eta = 1/r_m c_m - \alpha$$

$$\xi_k = \tfrac{1}{4}(r_e+r_i)\,c_m[y^2 + (2\pi r k)^2], \quad k = 0, 1, \ldots.$$

(ii) *Evaluation of the numerical functions*

The numerical functions $t(y)$, $t^*(y)$ and $y^*(t)$ of §4.1 are calculated in the following sequence. For a quantal secretion at location y: (1) obtain $t(y)$; (2) evaluate the potential at this point, $V_{max}(y) = V(y, t(y))$; (3) solve for t, the equation $V_{max}(y) - V(y,t) = \Delta_V$, the value of t being $t^*(y)$.

The functions $t(y)$ and $t^*(y)$ can be found numerically by Newton–Raphson methods, after obtaining analytical expressions for the derivatives. Although it is theoretically possible to obtain $y^*(t)$ by using direct numerical methods, it is computationally more convenient to obtain $y^*(t)$ by numerically solving $t^*(y) - t = 0$ for y, after having stored the values of $t^*(y)$ in an array.

APPENDIX B. PARAMETER ESTIMATION

(a) *Fusion-pore model*

There are four parameters used to specify the model, namely λ, γ, k and τ. A maximum likelihood procedure is used here to estimate the parameters.

Assume that there are $L+M+N$ pairs of observations (t_{1i}, t_{2i}) that have been partially sorted, such that L is the number of pairs with finite t_1 and finite t_2, M is the number of pairs with finite t_1 and infinite t_2 and N is the number of pairs with infinite t_1.

For the parameters $\boldsymbol{\theta} = (\lambda, \gamma, k, \tau)$ the likelihood of the sample is

$$\begin{aligned} L(\boldsymbol{\theta}; \boldsymbol{t}_1, \boldsymbol{t}_2) &= \prod_{i=1}^{L} f_T(t_1, t_2) \times \prod_{i=L+1}^{L+M} f_{T_1}(t_{1i})\, P(T_2 = \infty \mid T_1 = t_{1i}) \times [P(T_1 = \infty)]^N \\ &= \prod_{i=1}^{L+M} f_{T_1}(t_{1i}) \times \prod_{i=1}^{L} f_{T_2}(t_{2i} \mid t_{1i}) \times \prod_{i=L+1}^{L+M} P(T_2 = \infty \mid T_1 = t_{1i}) \times [P(T_1 = \infty)]^N, \end{aligned} \quad (14)$$

where the probability and density terms are as defined in equations (1, 2, 3, 4). Owing to the complexities of calculation of the derivatives and hessian matrix of the likelihood, a derivative-free version of Powell's quasi-Newton method was used to minimize $f(\boldsymbol{\theta}) = -\log L(\boldsymbol{\theta}; \boldsymbol{t}_1, \boldsymbol{t}_2)$ (FORTRAN code for this algorithm can be found in Press *et al.* (1986, p. 299)).

The likelihood maximization was done in two stages: (1) estimate λ, γ, k and τ from the likelihood of $\boldsymbol{t}_1$; (2) refine these estimates from the likelihood of $(\boldsymbol{t}_1, \boldsymbol{t}_2)$.

Based on the time until the first release, the likelihood of the sample for the parameters $\boldsymbol{\theta} = (\lambda, \gamma, k, \tau)$ is

$$L(\boldsymbol{\theta}; \boldsymbol{t}_1) = \prod_{i=1}^{L+M} f_{T_1}(t_{1i}) \times [P(T_1 = \infty)]^N. \quad (15)$$

All these parameters have a restricted space, either bounded by a lower value (zero) or between a range of values. To avoid working with a constrained maximization problem, it is more convenient to reparameterize the problem so that all parameters (and parameter estimates) have an unrestricted space (any real value). Hence, a reparameterization of

$$\phi = \left[\log\lambda, \log\gamma, \log k, \log\left(\frac{\tau}{t_{1(1)} - \tau}\right)\right]$$

was made where $t_{1(1)} = \min\{t_{1i}; i = 1, \ldots, L+M\}$, and $L(\phi)$ maximized.

(b) *Detection error model*

For this model, it is assumed that the 'window' width for observations, Δ_y, is known, and that k is set at five. So there are five parameters to estimate in the random-detection error model, λ, γ, τ, α and Δ_V. The likelihood of the sample for the parameters $\boldsymbol{\theta} = (\lambda, \gamma, \tau, \alpha, \Delta_V)$ is the same as in (14), but using the

PHILOSOPHICAL TRANSACTIONS OF THE ROYAL SOCIETY B BIOLOGICAL SCIENCES

density and probability terms in equations (1, 2, 6 and 7). The parameters are estimated numerically in the following stages:

(1) estimate λ, γ and τ from the likelihood of $\boldsymbol{t}_1$;

(2) estimate α and Δ_V from the likelihood of $\boldsymbol{t}_2$ given $\boldsymbol{t}_1$, with the values of λ, γ and τ from above;

(3) refine all these estimates from the likelihood of $(\boldsymbol{t}_1, \boldsymbol{t}_2)$.

In the first step, the likelihood $L(\boldsymbol{\theta}_1; \boldsymbol{t}_1)$ maximized is that in (15), where $\boldsymbol{\theta}_1 = (\lambda, \gamma, \tau)$. The second step maximized the likelihood

$$L(\boldsymbol{\theta}_2; \boldsymbol{t}_2 \mid \boldsymbol{t}_1) = \prod_{i=1}^{L} f^*_{T_2}(t_{2i} \mid t_{1i}) \times \sum_{i=L+1}^{L+M} P^*(T_2 = \infty \mid T_1 = t_{1i}),$$

where $\boldsymbol{\theta}_2 = (\alpha, \Delta_V)$. Note that

$$L(\boldsymbol{\theta}_1; \boldsymbol{t}_1)\, L(\boldsymbol{\theta}_2; \boldsymbol{t}_2 \mid \boldsymbol{t}_1) \leqslant L(\boldsymbol{\theta}; \boldsymbol{t}_1, \boldsymbol{t}_2),$$

so that a comparison of $L(\boldsymbol{\theta}_1; \boldsymbol{t}_1)\, L(\boldsymbol{\theta}_2; \boldsymbol{t}_2 \mid \boldsymbol{t}_1)$ with $L(\boldsymbol{\theta}; \boldsymbol{t}_1, \boldsymbol{t}_2)$ can be used to assess how effective the third (refinement) step has been.

(*c*) *Combined model*

In the combined model, six parameters are used, namely λ, γ, τ, α, Δ_V and v. The likelihood of the sample for the parameters $\boldsymbol{\theta} = (\lambda, \gamma, \tau, \alpha, \Delta_V, v)$ is again that given in equation (14), but with use of the probability and density terms that are as defined in equations (1, 2, 8, 9). A three stage method will again be used for parameter estimation, namely:

(1) estimate λ, γ and τ from the likelihood of $\boldsymbol{t}_1$;

(2) estimate α, Δ_V and v from the conditional distribution of the second releases;

(3) refine estimates of all parameters by using times of both first and second releases.

A reparameterization is again done to allow an unconstrained maximization to be made. Note that v can be no more than the inverse of the maximum interval between first and second releases, since the entire strip would always be covered by then. In addition, v cannot be negative. To achieve these constraints, v was reparameterized via a logistic type transformation as

$$v' = \log\left[v/(s_{1(L)}^{-1} - v)\right],$$

where $s_{1(L)} = \max\{s_{1i}; i = 1, \ldots, L\}$.

It is seen that v is estimated as zero whenever the likelihood (as a function of v) has a non-positive slope as $v \to 0$ $(v' \to -\infty)$, that is, whenever the sum of the scores

$$\frac{\partial}{\partial v} \log L(v; \boldsymbol{t}_2 \mid \boldsymbol{t}_1)\bigg|_{v=0} \leqslant 0.$$

So, in the second of the three stages, the total score at $v = 0$ is evaluated first (by using initial estimates of α and Δ_V) to see if $\hat{v} = 0$ (as indicated by a negative value of this derivative). When $\hat{v} = 0$ is indicated by this preliminary procedure, α and Δ_V can be estimated by setting $v = 0$ (and fitting a detection error model only); otherwise the likelihood needs to be maximized over $\boldsymbol{\theta} = (\alpha, \Delta_V, v)$. It speeds up the computation considerably if $\hat{v}$ is assumed zero.

APPENDIX C. PARAMETRIC BOOTSTRAP OF PARAMETER ESTIMATES

Once parameter estimates for a data set are obtained, pseudo-data may be simulated from the distribution with the estimates taken as the true parameters. The simulation method used here is based on that of Bennett & Robinson (1990). The bootstrap procedure is summarized as follows:

(1) obtain maximum likelihood estimates from the actual time course data, $\hat{\boldsymbol{\theta}}$;

(2) generate $L+M+N$ random pairs of release times from the $F_T(\boldsymbol{t}; \hat{\boldsymbol{\theta}})$ distribution;

(3) obtain new maximum likelihood estimates, $\hat{\boldsymbol{\theta}}^*_j$;

(4) repeat steps 2 and 3 for $j = 1, \ldots, N_{\mathrm{bs}}$;

(5) obtain empirical means, standard errors, bias etc. of the parameter estimates.

This method was applied to the combined model, generating pseudo-data with use of the parameter estimates obtained in this analysis (sets of $L+M+N = 800$ quantal secretion times). The estimation procedure was then applied to each simulated data set, and the results shown in table 2. Ideally, the number of bootstrap samples (N_{bs}) would be at least 1000. However, because of the intensive computing required for these procedures, the procedure was only repeated 200 times to obtain the bootstrap distribution of $(\hat{\lambda}, \hat{\gamma}, \hat{\Delta}_V)$, and ten times to obtain the bootstrap distribution of $(\hat{\lambda}, \hat{\gamma}, \hat{\tau}, \hat{\Delta}_V, \hat{v})$.

REFERENCES

Almers, W. 1990 Exocytosis. *A. Rev. Physiol.* **52**, 607–624.

Almers, W., Breckenridge, L. J. & Spruce, A. E. 1989 The mechanism of exocytosis during secretion in mast cells. *Soc. gen. Physiol.* **44**, 269–282.

Alvarez de Toledo, G., Fernández-Chacón, R. & Fernández, J. M. 1993 *Nature, Lond.* **363**, 554–558.

Augustine, G. J. & Charlton, M. P. 1986 Calcium-dependence of presynaptic calcium current and post-synaptic response at the squid giant synapse. *J. Physiol., Lond.* **381**, 619–640.

Baldo, G. J., Cohen, I. S. & Van der Kloot, W. 1986 Estimating the time course of evoked quantal release at the frog neuromuscular junction using end-plate current latencies. *J. Physiol., Lond.* **374**, 503–513.

Barrett, E. F. & Stevens, C. F. 1972*a* Quantal independence and uniformity of presynaptic release kinetics at the frog neuromuscular junction. *J. Physiol., Lond.* **227**, 665–689.

Barrett, E. F. & Stevens, C. F. 1972*b* The kinetics of transmitter release at the frog neuromuscular junction. *J. Physiol., Lond.* **227**, 691–708.

Bennett, M. R. & Fisher, C. 1977 The effect of calcium ions on the binomial parameters that control acetylcholine release during trains of nerve impulses at amphibian neuromuscular synapses. *J. Physiol., Lond.* **271**, 673–698.

Bennett, M. R., Fisher, C., Florin, T., Quine, M. P. & Robinson, J. 1977 The effect of calcium ions and temperature on the binomial parameters that control acetylcholine release by a nerve impulse at amphibian neuromuscular synapses. *J. Physiol., Lond.* **271**, 641–672.

PHILOSOPHICAL TRANSACTIONS OF THE ROYAL SOCIETY B BIOLOGICAL SCIENCES

Bennett, M. R. & Florin, T. 1974 A statistical analysis of the release of acetylcholine at newly formed synapses in striated muscle. *J. Physiol., Lond.* **238**, 93–107.

Bennett, M. R., Florin, T. & Hall, R. 1975 The effect of calcium ions on the binomial statistic parameters which control acetylcholine release at synapses in striated muscle. *J. Physiol., Lond.* **247**, 429–446.

Bennett, M. R., Jones, P. & Lavidis, N. A. 1986 The probability of quantal secretions along visualized terminal branches at amphibian (*Bufo marinus*) neuromuscular synapses. *J. Physiol., Lond.* **379**, 257–274.

Bennett, M. R. & Lavidis, N. A. 1979 The effect of calcium ions on the secretion of quanta evoked by an impulse at nerve terminal release sites. *J. gen. Physiol.* **74**, 429–456.

Bennett, M. R. & Lavidis, N. A. 1989 The probability of quantal secretion at release sites in different calcium concentrations in toad (*Bufo marinus*) muscle. *J. Physiol., Lond.* **418**, 219–233.

Bennett, M. R. & Robinson, J. 1990 Probabilistic secretion of quanta from nerve terminals at synaptic sites on muscle cells: non-uniformity, autoinhibition and the binomial hypothesis. *Proc. R. Soc. Lond.* B **239**, 329–358.

D'Alonzo, A. J. & Grinnell, A. D. 1985 Profiles of evoked release along the length of frog motor nerve terminals. *J. Physiol., Lond.* **259**, 235–258.

del Castillo, J. & Katz, B. 1956 Localization of active spots within the neuromuscular junction of the frog. *J. Physiol., Lond.* **132**, 630–649.

Delcour, A. H., Lipscombe, D. & Tsien, R. W. 1993 Multiples modes of N-type calcium channel activity distinguished by differences in gating kinetics. *J. Neurosci.* **13**, 181–194.

Dodge, F. A. & Rahamimoff, R. 1967 Co-operative action of calcium ions in transmitter release at the neuromuscular junction. *J. Physiol., Lond.* **193**, 419–432.

Efron, B. & Tibshirani, R. 1986 Bootstrap methods for standard errors, confidence intervals, and other measures of statistical accuracy. *Statist. Sci.* **1**, 54–77.

Fatt, P. & Katz, B. 1951 An analysis of the end-plate potential recorded with an intra-cellular electrode. *J. Physiol., Lond.* **115**, 320–370.

Gage, P. W. & Armstrong, C. M. 1968 Miniature end-plate currents in voltage-clamped muscle fibre. *Nature, Lond.* **218**, 363–365.

Hodgkin, A. L. & Nakajima, S. 1972 The effect of diameter on the electrical constants of frog skeletal muscle fibres. *J. Physiol., Lond.* **221**, 121–136.

Hodgkin, A. L. & Rushton, W. A. H. 1946 The electrical constants of a crustacean nerve fibre. *Proc. R. Soc. Lond.* B **133**, 449–479.

Jack, J. J. B., Noble, D. & Tsien, R. W. 1975 *Electric current flow in excitable cells*. Oxford: Clarendon.

Johannes, L., Lledo, P.-M., Roa, M., Vincent, J.-D., Henry, J.-P. & Datchen, F. 1994 The GTPase Rab3a negatively controls calcium-dependent exocytosis in neuroendocrine cells. *EMBO J.* **13**, 2029–2037.

Jones, S. V. 1987 Presynaptic mechanisms at vertebrate neuromuscular junctions. In *The vertebrate neuromuscular junction* (ed. M. M. Salpeter), pp. 187–295. New York: A. R. Liss.

Katz, B. 1969 The release of neural transmitter substances. *The Sherrington Lectures*, **X**. Liverpool: Liverpool University Press.

Katz, B. & Miledi, R. 1965*a* The measurement of synaptic delay, and the time course of acetylcholine at the neuromuscular junction. *Proc. R. Soc. Lond.* B **161**, 483–495.

Katz, B. & Miledi, R. 1965*b* The effect of temperature on the synaptic delay at the neuromuscular junction. *J. Physiol., Lond.* **181**, 656–670.

Monck, J. R. & Fernández, J. M. 1992 The exocytotic fusion pore. *J. Cell. Biol.* **119**, 1395–1404.

Monk, J. R. & Fernández, J. M. 1994 The exocytotic fusion-pore and neurotransmitter release. *Neuron* **12**, 707–716.

Nanavati, C., Markin, V. S., Oberhauser, A. F. & Fernández, J. M. 1992 The exocytotic fusion pore modelled as a lipidic pore. *Biophys. J.* **63**, 1118–1132.

Neher, E. 1993 Secretion without full fusion. *Nature, Lond.* **363**, 497–498.

Oberhauser, A. F., Monck, J. R. & Fernández, J. M. 1002 Events leading to the opening and closing of the exocytotic fusion pore have markedly different temperature dependencies. *Biophys. J.* **61**, 800–809.

Parnas, H., Havov, G. & Parnas, I. 1989 Effect of Ca^{2+} diffusion on the time course of neurotransmitter release. *Biophys. J.* **55**, 859–874.

Popov, S. V. & Poo, M. 1993 Synaptotagmin: a calcium-sensitive inhibitor of exocytosis? *Cell* **73**, 1247–1249.

Press, W. H., Flannery, B. P., Teukolsky, S. A. & Vetterling, W. T. 1986 *Numerical recipes. The art of scientific computing*. Cambridge: Cambridge University Press.

Stephens, M. A. 1963 Random walk on a circle. *Biometrika* **50**, 385–390.

Stevens, C. F. 1968 Synaptic physiology. *Proc. I.E.E.E.* **56**, 916–930.

Tuckwell, H. C. 1988 *Introduction to theoretical neurobiology*, vol. 1. *Linear cable structure and dendritic structure*. Cambridge: Cambridge University Press.

Ver der Kloot, W. 1988*a* Estimating the timing of quantal releases during end-plate currents at the frog neuromuscular junction. *J. Physiol., Lond.* **402**, 595–603.

Van der Kloot, W. 1988*b* The kinetics of quantal release during end-plate currents at the frog neuromuscular junction. *J. Physiol., Lond.* **402**, 605–626.

Wernig, A. 1972*a* Changes in statistical parameters during facilitation at the crayfish neuromuscular junction. *J. Physiol., Lond.* **226**, 751–759.

Wernig, A. 1972*b* The effects of calcium and magnesium on statistical release parameters at the crayfish neuromuscular junction. *J. Physiol., Lond.* **226**, 761–768.

Wernig, A. 1975 Estimates of statistical release parameters from crayfish and frog neuromuscular junctions. *J. Physiol., Lond.* **244**, 107–221.

Yamada, W. M. & Zucker, R. S. 1992 Time course of transmitter release calculated from simulations of a calcium diffusion model. *Biophys. J.* **61**, 671–682.

Yoshikami, D. & Okun, L. M. 1984 Staining of living presynaptic nerve terminals with selective fluorescent dyes. *Nature, Lond.* **310**, 53–56.

Zucker, R. S. 1973 Changes in the statistics of transmitter release during facilitation. *J. Physiol., Lond.* **229**, 787–810.

Zucker, R. S. & Fogelson, A. L. 1986 Relationship between transmitter release and presynaptic calcium influx when calcium enters through discrete channels. *Proc. natn. Acad. Sci. U.S.A.* **83**, 2032–2036.

Received 9 September 1994; revised 3 January 1995; accepted 19 January 1995

PHILOSOPHICAL TRANSACTIONS OF THE ROYAL SOCIETY B BIOLOGICAL SCIENCES